View metadata, citation and similar papers at core.ac.uk
brought to you by CORE
provided by Bilkent University Institutional Repository

SUBWAVELENGTH SURFACE PLASMON INTERFEROMETER FOR HIGH-THROUGHPUT SENSING

A THESIS

SUBMITTED TO THE DEPARTMENT OF PHYSICS

AND THE GRADUATE SCHOOL OF ENGINEERING AND SCIENCE

OF BILKENT UNIVERSITY

IN PARTIAL FULFILLMENT OF THE REQUIREMENTS

FOR THE DEGREE OF

MASTER OF SCIENCE

By

Özlem Yavaş

August, 2012

I certify that I have read this thesis and that in my opinion it is fully adequate, in scope and in quality, as a thesis for the degree of Master of Science.

_____

Asst. Prof. Dr. Coşkun Kocabaş

I certify that I have read this thesis and that in my opinion it is fully adequate, in scope and in quality, as a thesis for the degree of Master of Science.

_____

Prof. Dr. Atilla Aydınlı

I certify that I have read this thesis and that in my opinion it is fully adequate, in scope and in quality, as a thesis for the degree of Master of Science.

_____

Asst. Prof. Dr. Emrah Özensoy

Approved for the Graduate School of Engineering and Science:

_____

Prof. Dr. Levent Onural
Director of the Graduate School

ABSTRACT

SUBWAVELENGTH SURFACE PLASMON INTERFEROMETER FOR HIGH-THROUGHPUT SENSING

Özlem Yavaş

M.S. in Physics

Supervisor: Asst. Prof. Dr. Coşkun Kocabaş

August, 2012

Small detection volume, increased analysis speed and reduced cost are the main driving forces for miniaturized lab-on-a-chip systems. Subwavelength holes on opaque metal films provide a unique configuration for miniaturized sensors. Transmitted light through these tiny holes is governed by the electronic resonance on the surface of the metal film. Excitation of surface plasmon-polaritons (SPPs) on the metal-dielectric interface characterizes the resonance condition. The sensitive dependence of the plasmon resonance condition on the dielectric constant of the medium is used for label free sensing applications. In this thesis, we demonstrate a refractive index sensor based on a subwavelength plasmon interferometer using monochromatic light. Very high contrast fringe pattern is generated by the plasmon interferometer that consists of a sub-wavelength slit-groove pair with a small angle between them. The small angle between the groove and the slit provides spatially varying slit-groove distance which generates a high-contrast interference pattern. By interrogating the relative position of interference fringes, one can determine the refractive index of the dielectric medium on the metal surface. The presented plasmon interferometer provides a practical yet sensitive refractive index measurement scheme with very small detection volume.

Keywords: surface plasmon resonance sensors, plasmon interferometer, refractive index sensor, microfluidics.

ÖZET

DALGABOYU ALTI YÜZEY PLAZMON İNTERFEROMETRESİ

Özlem Yavaş

Fizik, Yüksek Lisans

Tez Yöneticisi: Asst. Prof. Dr. Coşkun Kocabaş

August, 2012

Küçülen dedektör hacmi, artan analiz hızı ve maliyetin küçülmesi minyatürize mikro sensor sistemlerinin gelişmesindeki önemli etkenlerdir. Opak metal filmlerdeki dalgaboyu altı delikler minyatürize sensörler için benzersiz bir konfigürasyon sağlamaktadır. Bu küçük deliklerden ışığın iletimi metal film yüzeyindeki elektronik resonans tarafından kontrol edilir. Metal-dielektrik arayüzeylerinde yüzey plazmon polaritonlarının uyarımı rezonans şartını belirler. Plazmon rezonans koşulunun ortamın dielektrik sabitine karşı duyarlı oluşu, etiketlemeden sensing uygulamalarında kullanılır. Bu tezde, monokromatik ışık kullanan dalgaboyu altı plazmon interferometresi tabanlı bir kırınım indisi sensörü sunuyoruz. Dalgaboyu altı boyutta aralarında küçük bir açı bulunan aralık-oluk çifti içeren plazmonik interferometre tarafından çok yüksek kontrast girişim deseni oluşturulur. Aralık ve oluk arasındaki küçük açı aralarınında değişken bir mesafe olmasını sağlar. Bu mesafenin kazandırdığı faz farkı sayesinde yüksek kontrast girişim deseni oluşur. Girişim saçaklarının birbirine gore pozisyonları ölçülerek metal yüzeyin üzerindeki ortamın kırınım indisi ölçülür. Bu tezde sunulan plazmon interferometresi çok küçük dedektör hacmi ile çok pratik ve duyarlı bir ölçüm tekniği sağlamaktadır.

Anahtar sözcükler: yüzey plazmon rezonans sensörleri, plazmon interferometresi, kırınım indisi sensörü, mikroakışkan.

Acknowledgement

First, I would like to express my deepest gratitude to Asst. Prof. Dr. Coşkun Kocabaş. His supportive and motivating attitude has continuously helped me and his constructive critics guided me during two years of my research period. Without his guidance I would have never succeeded in finishing this thesis work.

I would also present my gratitude to Prof. Dr. Atilla Aydınlı and Prof. Dr. Emrah Özensoy for their judgments and helpful critics as the Master's Thesis committee.

I owe my deepest gratitude to my parents Ayşe and Ömer Yavaş for their care and support. Without their love I would not be able to write any of these lines.

I would also like to thank my best friends "Semirsan" (Semih Kaya) and "Nurbaka" (Nurbek Kakenov) for being my 'psychological support unit' during my two years in Bilkent. Their existence made Bilkent years memorable, productive and valuable.

Finally, I would like to thank Volkan Uslu for being my brother. Without his destructions, this work might have been presented earlier. Nevertheless, it was worth every second of long chats and fun that we had.

This thesis is dedicated to a very special man, my grandfather, who had a never ending enthusiasm and love towards science and belief in my success all the time.

Contents

List of Figures

to my grandfather

Chapter 1

Introduction

Surface plasmon resonance (SPR) is the collective oscillations of the free electrons that are excited by an external electric field at the metal-dielectric boundary. Widely used SPR excitation schemes such as prism coupling and grating coupling are introduced in the 1960s. The surface plasmon resonance (SPR) sensors use the fact that the resonance condition of the oscillations of the free electrons is highly related to the changes in the dielectric constant of the medium. SPR based sensors attracted attention for chemical and biological sensing since early 1980s. In 1980 Gordon et al. had used the SPR to detect processes at metal surfaces [1]. Starting with this study many SPR sensors are presented which used different excitation schemes and different optical and geometrical configurations. Different sensing methods and signal interrogations such as intensity, wavelength and phase interrogation methods are presented with different geometries to increase the sensitivity of detection. Now, SPR sensors are widely used for label free detection and analysis of biomolecular and chemical interactions on metal surfaces. The benefits of these lab-on-a-chip sensors include small detection volume, high analysis speed and low cost.

In 1998 Ebbesen et al. observed that the transmission through subwavelength apertures is higher than predicted by the classical model [2]. Observation of the extraordinary transmission leaded the studies of subwavelength hole arrays as SPR sensors [3, 4] and plasmon interferometers [5-8]. Recently the studies on

plasmon interferometry provided highly sensitive and practical scheme for sensing. Various configurations of parallel slit and groove pairs were used in the previously presented plasmon interferometers [5]. The spectral analysis of the transmitted light enables the label free detection of the variations on the surface. The spectrum measurements require wavelength tunable source or a spectrometer. These requirements adversely affect the practicality of the sensors.

In this thesis we present a subwavelength plasmon interferometer for refractive index sensing which operates with a monochromatic light i.e. does not require any spectral analysis. The sensor does not require any bulky prism or grating structure to excite SPPs. This work presents a very practical sensing method based on the examination of the interference pattern by a simple image processing. The plasmon interferometer is integrated with a microfluidic channel to decrease the detection volume up to around 100fL.

1.2. Organization of the Thesis

In this thesis a subwavelength surface plasmon interferometer for high-throughput refractive index sensing is presented. The results of the test measurements are given and compared with the Matlab simulations. The physics lying behind surface plasmon interferometers and a brief review is also given in the first chapters of the thesis.

In chapter 1, an introduction to the field of surface plasmon resonance(SPR) sensors is made and the motivation of the work on our plasmon interferometer is given.

In chapter 2, the fundamentals of surface plasmon polariton (SPP) are presented starting from the Maxwell equations. The SPP excitation schemes are discussed.

Chapter 3 summarizes the concept and properties of SPR sensors as well as the performance characteristics of these sensors. Different interrogation methods that are used in SPR sensors are also explained.

Chapter 4 is a detailed review of the extraordinary transmission from subwavelength apertures and the applications based on this transmission property.

In chapter 5, we present the subwavelength plasmon interferometer which we have used for refractive index sensing. The results of the measurements and comparison with the theoretical calculations are given.

Chapter 6 provides a summary of the thesis. Some suggestions on further studies are also discussed.

Chapter 2

Surface Plasmon Polaritons

Surface plasmons are the collective oscillations of the electrons at the interface of two media with dielectric functions of opposite sign such as metal-dielectric interface. The coupling of electromagnetic waves to these oscillations of the electron plasma of the metal results in the excited modes propagating at the interface, called surface plasmon polaritons. To understand the nature of the surface plasmons we should first understand the optical properties of metals.

2.1. Optical Properties of Metals

The oscillation of free electrons and the interband transitions of the metals define the properties of metals and thus the surface plasmons. The dielectric function of the metal strongly depends on the frequency of the incoming electromagnetic wave. This strong dependence causes variety of optical phenomena. At frequencies up to the visible light (i.e. microwave and far infrared), it is well known that metals are highly reflective and the amount of the electromagnetic field that can penetrate into the metal is negligible. However for the near infrared and visible frequencies this penetration increases and for higher frequencies as ultraviolet region of the spectrum, the metal shows dielectric character which results in the well known ultraviolet transparency. For the noble metals, the interband transitions lead to strong absorption which is going to be discussed later in section 2.1.2. These phenomena are the results of the complex dielectric function of the metals [9].

2.1.1. Drude model

The Lorentz model of dipole oscillations model the response of electrons to an applied electric field as damped harmonic oscillations with equation of motion given as:

$$m\ddot{x} + m\gamma\dot{x} + m\omega_0^2 x = -eE_0 e^{-i\omega t} \tag{2.1}$$

where m and e are the mass and the charge of an electron and x is the displacement of the electron under the AC electromagnetic field $E(t) = E_0 e^{-i\omega t}$ with amplitude of E_0 and frequency of ω. The second term represents the frictional damping force with $\gamma = v_F/l = 1/\tau$ where v_F is the Fermi velocity and l is the electron's mean free path. τ is the relaxation time of the free electron gas. In the third term, ω_0 is the resonance frequency of the oscillation of the electron.

Drude model considers that the valance electrons of the metal are free electrons so that they experience no restoring force and the resonance frequency is almost zero. Thus the Drude model for a free electron with a mass of m_e reads;

$$m_e\ddot{x} + m_e\gamma\dot{x} = -eE_0 e^{-i\omega t} \tag{2.2}$$

The particular solution to this equation is $x = x_0 e^{-i\omega t}$ and by substituting into (1.2) it gives:

$$x(t) = \frac{e}{m_e(\omega^2 + i\gamma\omega)} E(t) \tag{2.3}$$

The polarization P of the free electron gas is given as $-Nex$ where N is the number of electrons per unit volume.

$$P = -\frac{Ne^2}{m_e(\omega^2 + i\gamma\omega)} E \tag{2.4}$$

The electric displacement is related to the polarization by;

$$D = \varepsilon_0 E + P \tag{2.5}$$

which is from the constitutive relation also equal to;

$$D = \varepsilon_0 \varepsilon E \tag{2.6}$$

Combining (2.4), (2.5) and (2.6);

$$\varepsilon_0 \varepsilon E = \varepsilon_0 E - \frac{Ne^2}{m_e(\omega^2 + i\gamma\omega)} E$$

$$\varepsilon(\omega) = 1 - \frac{Ne^2}{\varepsilon_0 m_e} \frac{1}{(\omega^2 + i\gamma\omega)}$$

$$\varepsilon_{Drude}(\omega) = 1 - \frac{\omega_p^2}{(\omega^2 + i\gamma\omega)} \tag{2.7}$$

where ω_p is the bulk plasma frequency which is equal to $\sqrt{Ne^2/\varepsilon_0 m_e}$. The complex dielectric function $\varepsilon_{Drude}(\omega) = \varepsilon_1 + i\varepsilon_2$ has real and imaginary parts as follows;

$$\varepsilon_1(\omega) = 1 - \frac{\omega_p^2}{(\omega^2 + \gamma^2)}$$

$$\varepsilon_2(\omega) = \frac{\gamma\omega_p^2}{\omega(\omega^2 + \gamma^2)} \tag{2.8}$$

The complex refractive index $\tilde{n}(\omega) = n(\omega) + i\kappa(\omega)$ of the medium is defined as $\tilde{n}(\omega) = \sqrt{\varepsilon}$ which gives [9];

$$\varepsilon_1 = n^2 - \kappa^2 \tag{2.9}$$

$$\varepsilon_2 = 2n\kappa \tag{2.10}$$

$$n^2 = \frac{\varepsilon_1}{2} + \frac{1}{2}\sqrt{{\varepsilon_1}^2 + {\varepsilon_2}^2} \tag{2.11}$$

$$\kappa = \frac{\varepsilon_2}{2n} \tag{2.12}$$

$\kappa(\omega)$ gives the electromagnetic wave absorption through the medium and it is related to the attenuation coefficient α of the Beer's law ($I(x) = I_0 e^{-\alpha x}$).

$$\alpha(\omega) = \frac{2\kappa(\omega)\omega}{c} \tag{2.13}$$

Thus, the imaginary part of the dielectric function describes the amount of absorption inside the medium. By using the real and imaginary components calculated by Drude model (2.8), it can easily be seen that for low frequencies that satisfy $\omega \ll \tau^{-1}$ the imaginary part of the dielectric function is larger than the real part. Thus, the real and imaginary parts of the index of refraction are approximately equal which yields $n \approx \kappa = \sqrt{\varepsilon_2/2}$ and using (2.13);

$$\alpha(\omega) = \frac{2\omega\sqrt{\varepsilon_2/2}}{c} = \left(\frac{2\omega\omega_p^2}{\gamma c^2}\right)^{1/2} = \sqrt{2\sigma_0\omega\mu_0} \tag{2.14}$$

where $\sigma_0 = Ne^2\tau/m_e = \omega_p^2\tau\varepsilon_0$ is the dc conductivity. The power of the field falls off as $e^{-2z/\delta}$ as the field strength varies as $e^{-z/\delta}$. Comparing this type of a field with the field of the Beer's law the skin depth is obtained;

$$\delta = \frac{2}{\alpha} = \left(\frac{2\gamma c^2}{\omega\omega_p^2}\right)^{1/2} = \sqrt{\frac{2}{\sigma_0\omega\mu_0}} \tag{2.15}$$

In the visible region of the electromagnetic spectrum where $\omega/2\pi \sim 10^{15}$Hz, usually $\omega \gg \gamma$, since γ is typically of order 10^{-14}s. Therefore the damping is negligible in (2.8) yielding a predominantly real dielectric function;

$$\varepsilon(\omega) = 1 - \frac{\omega_p^2}{\omega^2} \tag{2.16}$$

From the relation of dielectric constant with refractive index $\tilde{n}(\omega) = \sqrt{\varepsilon}$ it is obvious that $\tilde{n}(\omega)$ is imaginary for $\omega < \omega_p$, zero for $\omega = \omega_p$ and real for $\omega > \omega_p$ [10]. The reflectivity R of the metal is

$$R = \left|\frac{\tilde{n}-1}{\tilde{n}+1}\right|^2 \tag{2.17}$$

From which we can conclude that the reflectivity of metals is 100% for the frequencies up to ω_p. So with the ω_p in the ultraviolet metals are very good reflectors at visible frequencies. The dielectric function (2.16) changes sign as ω goes through ω_p which means that the reflectivity decreases after $\omega = \omega_p$ point in the regime of $\omega > \omega_p$ where the transmittance increases. So at the ultraviolet frequencies metals are transparent which is known as ultraviolet transparency of metals.

2.1.2. Interband Transitions

Drude model gives good results for the optical properties of metals in the infrared regime by only considering the free electron oscillations, where the energy of photon is smaller than the threshold of interband transitions of the metal. However for some of the noble metals the interband transitions should be taken into account since the interband transitions start to occur for energies larger than 1eV. For a wavelength shorter than ~550 nm, the increase of imaginary component of the dielectric function of gold is stronger than the value expected by the Drude model. If the incoming photons have higher energy than the respective band thresholds, they cause electron transitions from the filled band below the Fermi level to higher energy levels. Therefore to get more precise results, the response of bound electrons should also be taken into account. This approach corresponds to the Lorentz model described in equation (2.1) where m is the effective mass of the bound electron which is slightly different than the effective mass of the free electron and $m\omega_0$ is the restoring force constant. The bound electron has the resonance frequency of ω_0. By using the same ansatz as in the free electron case, we obtain the dielectric function as follows:

$$\varepsilon_{interband}(\omega) = 1 + \frac{\tilde{\omega}_p^2}{(\omega_0^2 - \omega^2) - i\gamma\omega} \tag{2.18}$$

$\varepsilon_{interband}(\omega)$ has real and imaginary components (ε_1 and ε_2) as

$$\varepsilon_1 = 1 + \frac{\widetilde{\omega}_p^2(\omega_0^2 - \omega^2)}{(\omega_0^2 - \omega^2)^2 + \gamma^2\omega^2}$$

$$\varepsilon_1 = \frac{\gamma\widetilde{\omega}_p^2\omega}{(\omega_0^2 - \omega^2)^2 + \gamma^2\omega^2} \tag{2.19}$$

where $\widetilde{\omega}_p = \sqrt{\widetilde{N}e^2/m\varepsilon_0}$ in which $\widetilde{N}$ denotes the density of the bound electrons.

Free electron (2.7) and the interband transition (2.19) contributions should be added up to obtain the realistic model. The model then fits the experimental data for both the wavelengths below and above the transition threshold. In this section $\varepsilon_{interband}(\omega)$ is calculated considering only one transition. To get a better fit to any experimental data the higher order transitions should be taken into account. For example for gold one can take $\varepsilon_\infty = 6$ for the integrated higher order transition contributions.

2.2. Surface Plasmon Polaritons at Plane Interfaces

Surface plasmon polaritons are the electromagnetic surface wave modes resulting from the coupling of the electromagnetic fields to the oscillations of the free electrons of the metal. In this section Maxwell equations for the metal-dielectric interface will be solved to study the surface plasmon polariton properties. We consider a plane interface between two medium where one of the medium ($z < 0$ of the Cartesian coordinate system) is taken to have a general complex frequency dependent dielectric function $\varepsilon_1(\omega)$ and other medium ($z > 0$) is taken to have a real dielectric function $\varepsilon_2(\omega)$. Figure 2.1 shows the geometry to be considered.

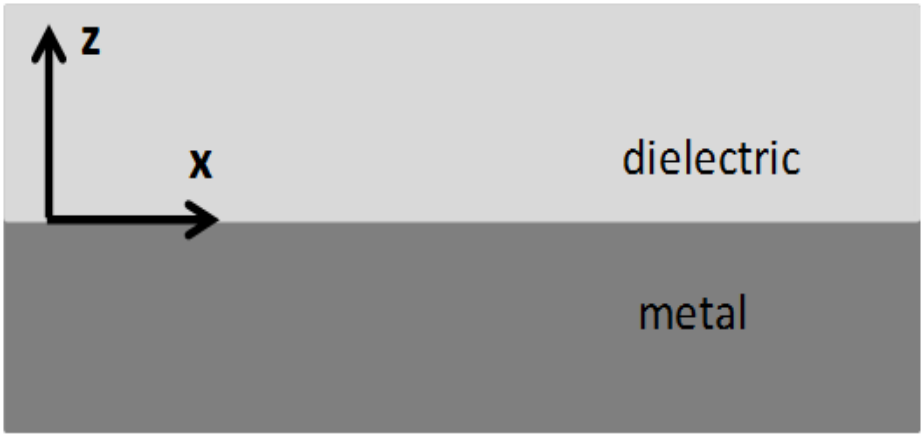

Figure 2.1 The geometry and coordinates that are to be considered in the calculations for the SPP propagation at metal dielectric interface

The Maxwell equations with no external excitation are

$$\begin{aligned} \nabla . D &= \rho_{ext} = 0 \\ \nabla . B &= 0 \\ \nabla \times E &= -\frac{\partial B}{\partial t} \\ \nabla \times H &= J_{ext} + \frac{\partial D}{\partial t} = \frac{\partial D}{\partial t} \end{aligned} \tag{2.20}$$

where D is the electric displacement, E is the electric field, H is the magnetic field and B is the magnetic flux density. External charge and current densities are taken to be zero. The fields are related to each other by constitutive relations

$$\begin{aligned} D &= \varepsilon_0 \varepsilon E \\ H &= \mu_0 \mu B \end{aligned} \tag{2.21}$$

Combining the last two equations in (2.20) and neglecting the changes in the dielectric profile $\varepsilon = \varepsilon(r)$ over distances of around one optical wavelength, the wave equation can be obtained as

$$\nabla^2 E - \frac{\varepsilon}{c^2}\frac{\partial^2 E}{\partial t^2} = 0 \tag{2.22}$$

where the $c^2 = 1/\mu_0\varepsilon_o$ relation is used. The solutions for the separate regions with different dielectric constants have to be matched using the appropriate boundary conditions. Including the AC nature of the electric field $E(r,t) = E(r)e^{-i\omega t}$ the wave equation becomes

$$\nabla^2 E - \varepsilon k_0^2 E = 0 \tag{2.23}$$

which is Helmholtz equation with $k_0 = \omega/c$, the wave vector of the propagating wave in vacuum. Since two media is considered to coincide at $z = 0$, if there is only propagation in the x direction (i.e. $\varepsilon = \varepsilon(r)$ and $E(x,y,z,t) = E(z)e^{i\beta x}e^{-i\omega t}$ where $\beta = k_x$ is the propagation constant of the travelling waves) the wave equation becomes

$$\frac{\partial^2 E(z)}{\partial z^2} - (\varepsilon k_0^2 - \beta^2)E = 0 \tag{2.24}$$

Same approach results in a similar wave equation for the magnetic field. Deriving the field components of $E$and H explicitly from the curl equations in (2.20) one can find a set of relations between the field components by also considering the propagation geometry (i.e. $\frac{\partial}{\partial y} = 0$ and $\frac{\partial}{\partial x} = i\beta$). Two sets of solutions for two different polarizations, transverse magnetic (TM or p) and transverse electric (TE or s) modes are obtained from that set. It is reasonable to consider here only the p-polarized waves since the s-polarized waves give no solution [9]. Thus the field components for p-polarization are for $z > 0$

$$\begin{aligned} H_y(z) &= A_2 e^{i\beta x}e^{-k_2 z} \\ E_x(z) &= iA_2\frac{1}{\omega\varepsilon_0\varepsilon_2}k_2 e^{i\beta x}e^{-k_2 z} \\ E_z(z) &= -A_1\frac{1}{\omega\varepsilon_0\varepsilon_2}k_2 e^{i\beta x}e^{-k_2 z} \end{aligned} \tag{2.25}$$

and for $z < 0$

$$\begin{aligned} H_y(z) &= A_1 e^{i\beta x} e^{-k_2 z} \\ E_x(z) &= iA_1 \frac{1}{\omega \varepsilon_0 \varepsilon_1} k_1 e^{i\beta x} e^{-k_1 z} \\ E_z(z) &= -A_1 \frac{1}{\omega \varepsilon_0 \varepsilon_1} k_1 e^{i\beta x} e^{-k_1 z} \end{aligned} \tag{2.26}$$

where k_1 and k_2 are the wave vectors normal to the interface and their reciprocals give the evanescent decay length of the fields that are normal to the interface [9].

The boundary conditions to be considered are the continuity of H_y, $\varepsilon_1 E_z$ and $\varepsilon_2 E_z$ which yields $A_1 = A_2$, $k_1/k_2 = -\varepsilon_1/\varepsilon_2$ and the relations for the wave vector components

$$\begin{aligned} k_1^2 &= \beta^2 - k_0^2 \varepsilon_1 \\ k_2^2 &= \beta^2 - k_0^2 \varepsilon_2 \end{aligned} \tag{2.27}$$

Combining all of these results the dispersion relation can be obtained

$$\beta^2 = k_x^2 = \frac{\varepsilon_1 \varepsilon_2}{\varepsilon_1 + \varepsilon_2} k_0^2 = \frac{\varepsilon_1 \varepsilon_2}{\varepsilon_1 + \varepsilon_2} \frac{\omega^2}{c^2} \tag{2.28}$$

Also the normal component of the wave vector in two media reads

$$k_j^2 = \frac{\varepsilon_j^2}{\varepsilon_1 + \varepsilon_2} k^2 \qquad j = 1,2 \tag{2.29}$$

The imaginary component of the complex dielectric function may be neglected at this point. Since the wave propagation is in the x direction the wave vector $\beta = k_x$ is required to be real. By examining (2.28) it is obvious that the sum and the product of the dielectric functions must be both negative or both positive. In addition to that condition to have the waves confined to the surface the denominator of the (2.29) must be negative so that k_j^2 is purely imaginary (i.e. the

normal component of the fields exponentially decay) [10]. Thus the conditions for the surface plasmon polariton to exist are:

$$\begin{aligned} \varepsilon_1 . \varepsilon_2 &< 0 \\ \varepsilon_1 + \varepsilon_2 &< 0 \end{aligned} \tag{2.30}$$

Thus one of the dielectric constants must be negative with an absolute value larger than that of the other. The surface plasmon polaritons exist only at the interface of two media with dielectric permittivities of opposite sign, i.e. metal dielectric surfaces as studied in this section. Metals such as gold and silver have large negative real component of the dielectric constant for visible wavelengths that makes them preferable for the surface plasmon studies.

2.2.1. Properties of Surface Plasmon Polaritons

Considering the imaginary part of the metal's dielectric function will provide solutions that include ohmic losses. The complex dielectric function ε_1 can be redefined as $\varepsilon_1 = \varepsilon_1^{'} + i\varepsilon_1^{''}$ and the dielectric medium is assumed to be a good dielectric with real dielectric function. The complex dielectric function yields a complex wave vector

$$k_x = k_x^{'} + ik_x^{''} \tag{2.31}$$

By inserting this complex wave vector into the (2.25) and (2.26) it can be stated that the real part $k_x^{'}$ determines the SPP wavelength and the imaginary part $k_x^{''}$ defines the damping of the SPP which propagates along the interface. By using the dispersion relation (2.28) and the assumption that $\left|\varepsilon_1^{''}\right| \ll \left|\varepsilon_1^{'}\right|$, the real and imaginary parts of the k_x are

$$k_x^{'} \approx \frac{\omega}{c}\sqrt{\frac{\varepsilon_1^{'}\varepsilon_2}{\varepsilon_1^{'}+\varepsilon_2}} \tag{2.32}$$

$$k_x^{''} \approx \frac{\varepsilon_1^{''}\varepsilon_2}{2\varepsilon_1^{'}(\varepsilon_1^{'}+\varepsilon_2)}\frac{\omega}{c}\sqrt{\frac{\varepsilon_1^{'}\varepsilon_2}{\varepsilon_1^{'}+\varepsilon_2}} \tag{2.33}$$

Thus,

$$\lambda_{SPP} = \frac{2\pi}{k_x^{'}} = \lambda \sqrt{\frac{\varepsilon_1^{'} + \varepsilon_2}{\varepsilon_1^{'}\varepsilon_2}} \tag{2.34}$$

Where λ is the wavelength of light in vacuum. 1/e intensity propagation length of the SPP for gold-air interface at 633nm wavelength is calculated as 10μm from $1/k_x^{''}$ where the dielectric function of gold is taken as $\varepsilon_1 = -11.6 + i1.2$ at that wavelength. The decay length for the z-components of the SPP for two media can also be obtained from (2.29) as,

$$k_1 = \frac{\omega}{c}\left[1 + \frac{i\varepsilon_1^{''}}{2\varepsilon_1^{'}}\right]\sqrt{\frac{\varepsilon_1^{'2}}{\varepsilon_1^{'} + \varepsilon_2}} \tag{2.35}$$

$$k_2 = \frac{\omega}{c}\sqrt{\frac{\varepsilon_2^{'2}}{\varepsilon_1^{'} + \varepsilon_2}}\left[1 + \frac{i\varepsilon_1^{''}}{2(\varepsilon_1^{'} + \varepsilon_2)}\right] \tag{2.36}$$

Neglecting the very small imaginary part of the complex dielectric function of the gold at 633nm the decay lengths in gold and air are 28nm and 328nm respectively from which it can be concluded that the SPP can travel more in the dielectric medium than in the metal.

2.3. Excitation of Surface Plasmon Polaritons

SPPs are the excited modes propagating at the interface of the two media with permittivities of opposite sign such as metal dielectric interface as considered in the previous sections. The SPP dispersion curve lies to the right of the light line since $\beta = k_x > k$ where k is the wave vector of light in the dielectric side. In order to excite SPPs the momentum and the energy conservation must be satisfied. The momentum mismatch between the light line and the SPP line must be overcome. So the excitation is prohibited for any frequency of incident light since at any incidence angle the x component of incident wave vector ($ksin\theta$) can not exceed the k_x of the SPP propagation (β). Some special techniques must be

used for phase matching. The most common techniques are prism coupling and grating coupling.

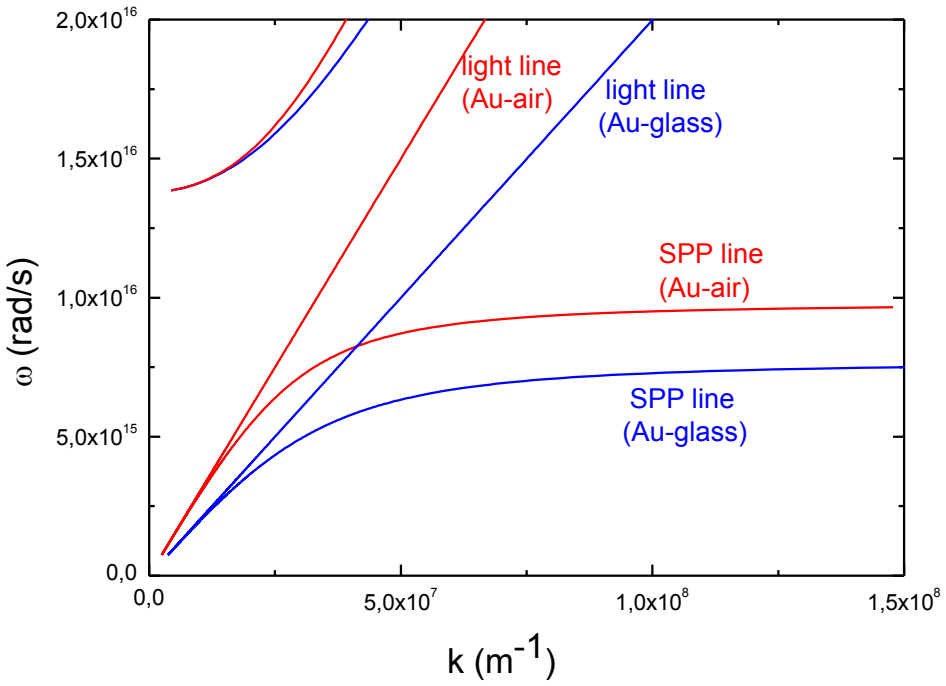

Figure 2.2 The dispersion relation for gold-air (red) and gold-glass (blue) interfaces calculated from the Drude model with parameters $\boldsymbol{\omega_p = 13.8 \times 10^{15} s^{-1}}$ and $\boldsymbol{\gamma = 1.075 \times 10^{14} s^{-1}}$ for gold.

There are two different geometries used for prism coupling (Fig. 2.3). In the most common configuration which is known as Kretschmann configuration [11] the metal thin film is evaporated on top of a glass prism where the incident light impinging from the prism has the x component of the wave vector $k_{x,i} = kn_{prism}sin\theta$ sufficient to excite SPPs at the metal dielectric interface by the penetration of the evanescent waves. It is important to note that the SPP phase matching condition at glass-metal interface cannot be achieved since the SPP dispersion for that interface lies to the right of the light line of the glass. (Fig. 2.2) Another similar configuration is Otto configuration[12] where this time there is a small dielectric gap between the metal and the prism and evanescent field tunnels through the dielectric to the metal-dielectric interface to excite SPPs. The SPP excitation is observed as a decrease in the reflected intensity.

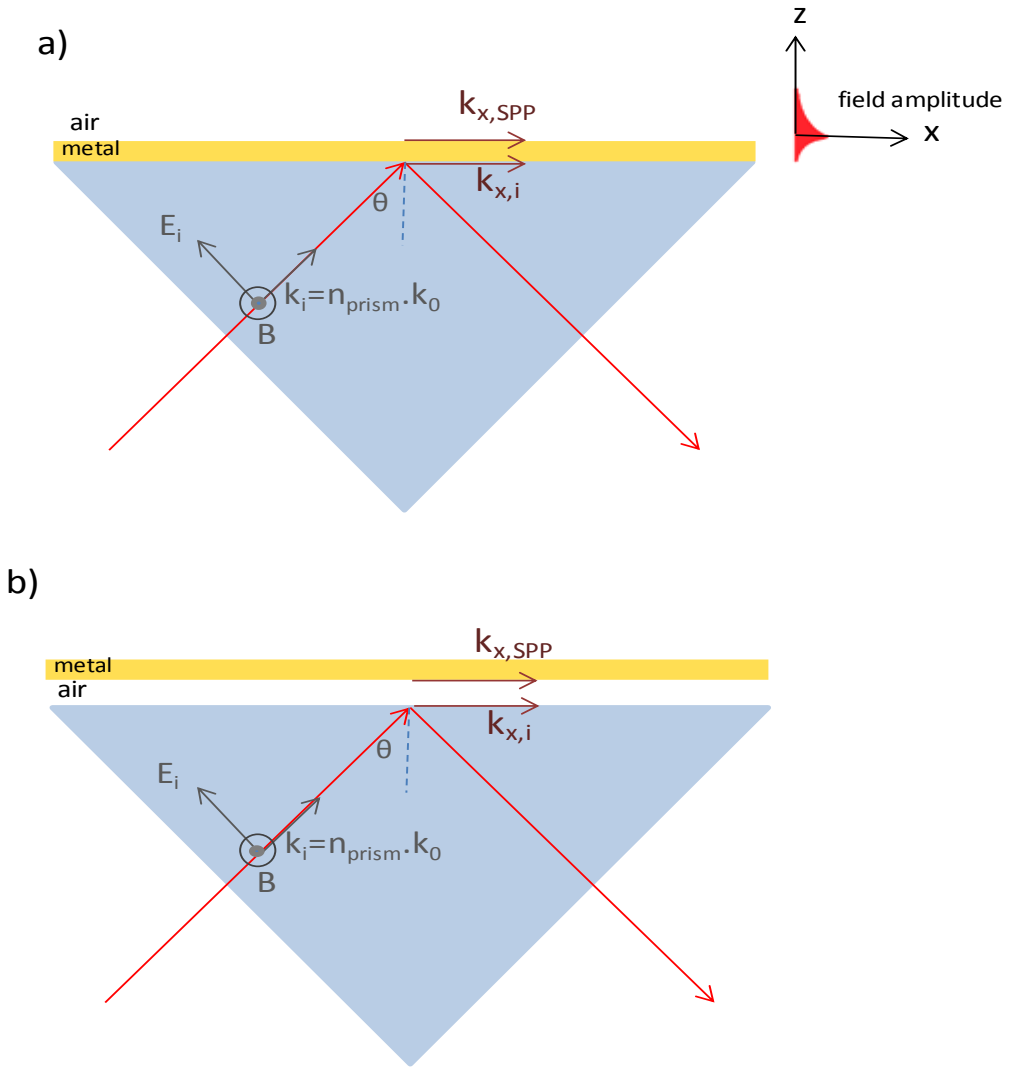

Figure 2.3 Kretschmann (a) and Otto (b) configurations of SPP excitation by prism coupling.

Fabricating grating structures on the metal surface (Fig. 2.4) is another widely used method to excite SPPs. Momentum necessary to overcome the mismatch is provided by the grating structure and it is related to the grating period a

$$\beta = k\,sin\theta \pm n\frac{2\pi}{a} \qquad n = 1,2,3,\ldots \tag{2.37}$$

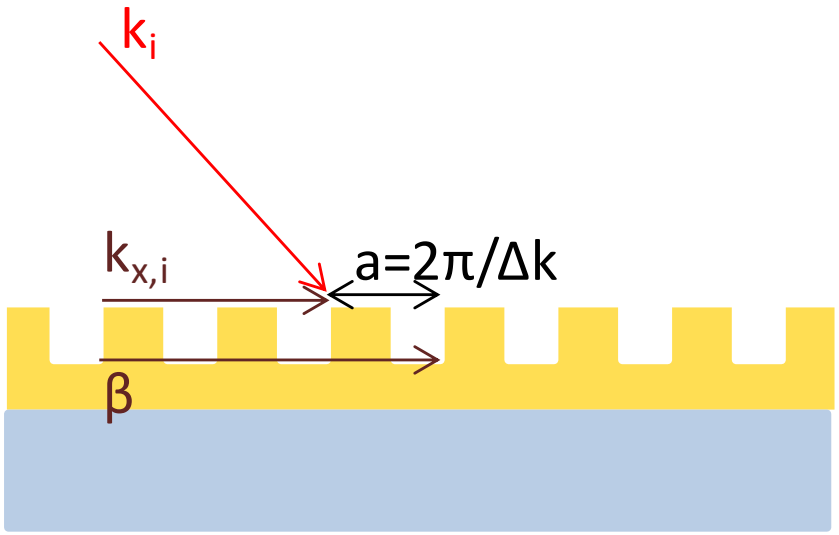

Figure 2.4 Schematic drawing of the grating coupling method for SPP excitation on metal surface.

Another well known method for SPP excitation is the waveguide coupling [13]. The propagating electromagnetic modes in the waveguide is coupled to the surface plasmons on the thin metal film, that is coated on the waveguide, as long as the wave constants are matched (i.e. the momentum mismatch is overcome).

Scattering from a sub wavelength ridge, groove, slit, hole or a roughness on the surface can also satisfy the condition where the parallel component of the diffracted k vector matches the surface plasmon wave vector which is parallel to the interface.

SPP generation and coupling by a groove (Fig. 2.5) has been studied by many groups [14-19]. When a groove has localized modes inside, the standing waves in the vertical direction (z-direction) which arise from the reflection at the bottom of the groove can couple to surface plasmon polaritons on the surface of two media. The maximum reflectivity depends on the groove depth, width and the wavelength of the incident light. For increasing wavelength the position of the high intensity of the standing wave moves towards the groove opening (upwards in z direction) and the enhancement of the field at the groove opening results in the efficient coupling to the SPP modes on the surface [19].

Exciting surface plasmon polaritons by using grooves are widely used in recent studies and sensors [5, 7] and the work that is presented in this thesis also uses a subwavelength groove to excite surface plasmons.

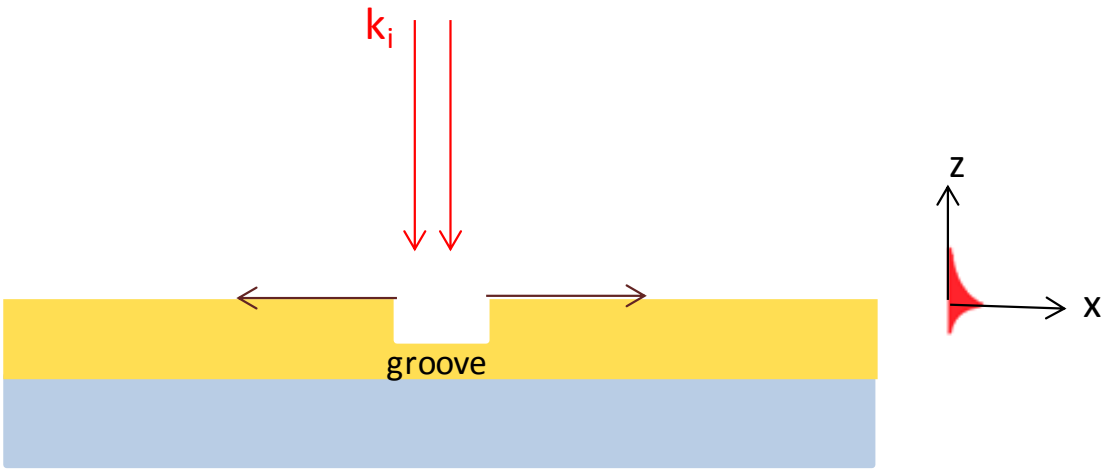

Figure 2.5 Schematic drawing of the excitation of the SPP by a single groove.

2.4. Localized Surface Plasmons

Localized surface plasmons (LSP) are non-propagating surface plasmon modes that are confined to the surface of metallic nanostructures such as nanoparticles where the free electrons couple to an electromagnetic field that result in a resonance. The curves on the surface of the nanostructure provide restoring force on the electron oscillations driven by an external electric field. The resonance situation yields the enhancement of the field inside and near field zone of the particle. Excitation of a LSP resonance on curved metallic nanostructures does not require phase matching. Therefore illumination of the surface by direct light leads resonantly enhanced absorption and scattering.

Chapter 3

Surface Plasmon Resonance Sensors

3.1. Introduction/concept of SPR sensors

Surface Plasmon Resonance (SPR) sensors are the sensors that benefit the specific phase matching resonance conditions that are required to excite the surface plasmon polariton waves. Since the SPPs are the wave modes propagating at the interface of the two media the wave vector which is related to the phase matching condition is extremely sensitive to changes on the boundary such as dielectric constant (index of refraction) changes due to adsorption of a molecule on the surface. Due to this extreme sensitivity SPR sensors are widely used for analyzing the chemical and biochemical reactions and molecular bindings. SPR biosensors have been used various fields such as food safety analysis, medical diagnostics and environmental monitoring.

Index of refraction is the determined quantity from optical interrogations of the SPR in these sensors. Since the change of the bulk properties of the dielectric medium will lead the changes of the index of refraction, the sensing scheme does not require labeling of the molecules. This property of SPR sensors enables the real time analysis of the biological and molecular interactions.

There are two conventional methods (prism coupling and grating) of excitation of surface plasmon polaritons that are mostly used in SPR sensors which are explained in the previous chapter. The Kretschmann geometry uses coupling of evanescent waves produced by the attenuated total internal reflection (ATR) of

incident light with surface plasmon and it is the most popular among the SPR sensors.

In the SPR sensor the quantity that is to be measured is the refractive index. The excitation of SPP is observed as the resonant absorption of the energy of the incident wave on the surface. Owing to this fact, the variations in the optical output parameters are interrogated to determine the refractive index changes. The sensor output can be coupling angle, wavelength, phase, intensity or polarization [13] according to the type and operation preferences of the sensor. Figure 3.1a shows an example of an SPR sensor that uses Kretschmann geometry. The sensor output that is the reflected intensity with respect to the angle of incidence is given in the Figure 3.1b. As the refractive index of the medium above the metal film changes, the excitation angle of the SPPs shifts. Measuring this shift, the variation of the refractive index can be detected.

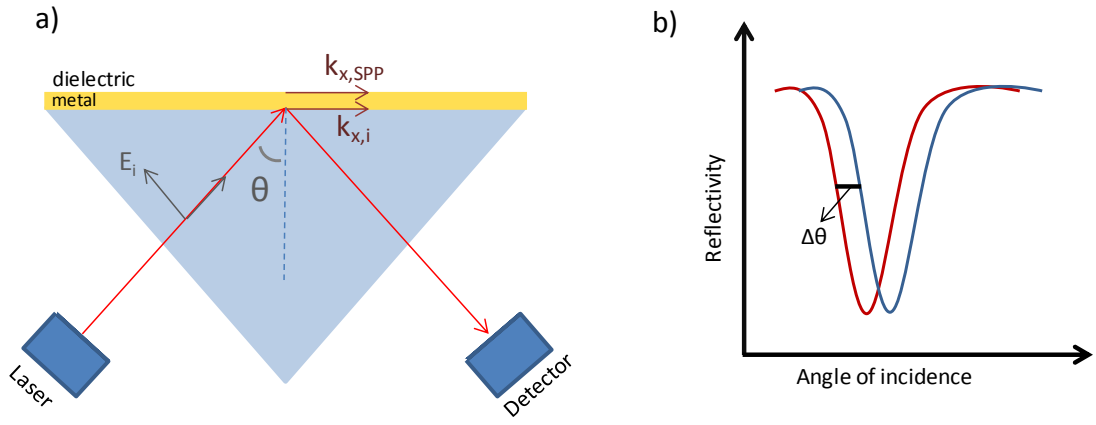

Figure 3.1 (a) Schematic of an SPR sensor based on Kretschmann configuration. (b) The reflected intensity profile with respect to the angle of incidence (θ). The excitation angle of the SPP shifts as the refractive index of the dielectric medium changes.

One of the widely used interrogation methods is angular modulation. The angular modulation based SPR sensors use monochromatic light. The sensor output is the

incidence angle at which the resonance condition is satisfied. Therefore the possible angular range is scanned to obtain the SPR excitation angle. Any change of refractive index will lead the shift of this angle allowing the detection of varying index of refraction [20-22].

Another interrogation method is wavelength modulation method. This time the angle of incidence is kept constant and the source is a collimated light with all the wavelengths in it. The wavelength at which the strongest coupling occurs is the resonance wavelength. Measuring the change of the resonance wavelength, change of refractive index can be determined [23, 24].

There are also intensity interrogated SPR sensors that measure the intensity of the reflected beam at which the resonance condition is satisfied by keeping the incidence angle and wavelength constant. The reflected intensity changes as the refractive index of the dielectric medium changes. So the intensity interrogation SPR sensors use this dependence to sense the refractive index variations [25-31].

The SPR sensors with phase and polarization modulation sense the variation of the phase and polarization as the refractive index changes [32, 33].

The most common SPR sensors use intensity, wavelength or angular [34, 35] interrogation methods.

3.2. Performance characteristics of SPR sensors

The performance of a SPR sensor can be tested in terms of the parameters that can be listed as sensitivity, linearity, resolution, accuracy, reproducibility, dynamic range, limit of detection and limit of quantification [13]. These are mainly related to the optical design of the SPR sensor.

The sensitivity of the SPR sensor is the derivative of the sensor output with respect to the quantity that is to be measured. Usually in SPR sensors the parameter to be measured is the refractive index (RI), n, thus;

$$S = \frac{\partial Y}{\partial n}$$

where Y is the measured output quantity.

The resolution of the SPR sensor is the smallest amount of change in the quantity to be determined that can be detected by the sensor. Resolution is a measure of the detector's ability to determine the SPR parameter that is to be measured. Thus, it depends on the detector noise, σ. The resolution of a sensor depends on the noise in the measured intensity of reflected light. The resolution R is defined as:

$$R = \frac{\sigma}{S}$$

The dynamic range of the sensor is the range of the values of the quantity to be measured that can be measured by the sensor.

The limit of detection (LOD) is the value of the quantity that is to be measured from the smallest output value that can be measured. It depends on the interactions between the analyte and the biorecognition element and the mass variation on the surface of the sensor.

The accuracy is the degree of closeness of the measured quantity to the actual value of that quantity. For a sensor usually it is defined as the percentage of the ratio of the error to the output. If the relation between the sensor output and the parameter that is measured (RI) is linear, the sensor is said to be linear which simplifies the calibration of the sensor. Most of the biosensors have non-linear response to the concentration of the analyte. The reproducibility of the sensor is the attainment degree of the sensor to the same results when the measurement is done multiple times.

Typical refractive index sensors with Kretschmann geometry that work with intensity modulation method have reported resolutions that are around 10^{-5} –

10^{-6} RIU (Refractive Index Unit). In 2006 Lechuga et al. used a multilayer structure where they have combined magneto-optic activity of the magnetic materials with SPR. They improved the sensitivity of the conventional SPR sensors from the order of 10^{-5} to 5×10^{-6} RIU [36]. Following the studies of angular or wavelength modulation based sensors with a prism coupler [37-39], the resolution of the commercial sensors have been improved down to 1×10^{-7} RIU by Biacore. Another prism coupled SPR sensor type is phase modulation based sensor. In 2004 Wu et al. presented a Mach-Zehnder interferometer where the interference of TM and TE polarized waves are formed. The sensor resolution was determined to be 5.5×10^{-8} [40].

Refractive index sensors that use grating coupling method for excitation of the SPPs are not as commonly used as the sensors which use prism coupling. Homola et. al. used grating coupling and angular spectroscopy based SPR sensor for refractive index measurements with a monochromatic light. They presented their resolution as 5×10^{-6} RIU [41]. Later Homola and Telezhnikova developed a different sensor where they used a polychromatic light incident on a grating structure. Using a position sensitive detector they detected the spectrum of the diffracted light. The sensor was reported to be available to measure refractive index changes as small as 3×10^{-7} RIU [42].

For the study of binding of large analytes or molecules on the surface, long range surface plasmon based sensors are presented to be very sensitive with resolutions around 3×10^{-8}RIU [43]. Long range surface plasmons are not sensitive to the changes in the surface as the surface plasmons. Their sensitivity is high for the farther regions from the surface when compared to short range surface plasmons. That is the reason they are used to sense large analytes.

A detailed comparison and analysis of the recent sensors that are used for food quality and safety measurements and medical diagnostics are presented in the review paper by Homola [44]. Among medical diagnostic purposed sensors the

lowest LOD that is used commercially is by Besselink et. al. using sensor system Ibis II [45]. Using prostate-specific antigen (PSA) as an analyte they established LOD as small as 0.15 ng/mL. For environmental monitoring Farre et. al. had presented LOD of their sensor system as 20 pg/mL [46].

Chapter 4

Plasmonic Interferometers

The SPR sensor that will be presented in this thesis is based on surface plasmon interference. There are many studies recently conducted on the surface plasmon interferometry [5-7, 47, 48]. Since SPPs are the electromagnetic waves propagating on a metallic surface, two surface plasmon waves can interfere constructively or destructively depending on their relative phase. The interference obtained in the presented sensor can be observed and interrogated owing to the extraordinary transmission of light through subwavelength slits which was first observed by Ebbesen et. al. in 1998 for a square array of circular apertures where SPPs play an important role.

To understand the physics behind the interferometer, the extraordinary transmission through subwavelength apertures and the previous applications of the observations of this extraordinary transmission phenomenon which are related to surface plasmon interferometry has to be understood.

4.1. Extraordinary transmission through subwavelength apertures

The interest in the transmission of radiation through thin conducting films has been initiated by the observation of Ebbesen et. al. in 1998. The extraordinary transmission phenomenon is observed through the subwavelength aperture arrays [2]. The studies based on the transmission followed that observation. Thin film is patterned with an array of holes [3, 4, 49-52] or a single hole that is surrounded by surface corrugations [3, 53] to enhance the transmission in some of these studies.

The transmission through an aperture involves diffraction phenomenon and it can be explained by some approximations of the classical diffraction theory. When the radius of a circular aperture, r, is larger than the wavelength of the incident light, λ_i, the Huygens-Fresnel principle, so the scalar diffraction theory by Kirchoff, can be used to understand the nature of the transmitted intensity. It is in the form of an Airy function pattern where a bright spot in the center is surrounded by concentric rings with decreasing intensity. The transmission coefficient T, which is the ratio of the transmitted intensity to the incident intensity, is approximately unity for an aperture where $r \gg \lambda_i$.

The surface plasmon polaritons are effective in the transmission for the subwavelength regime where $r \ll \lambda_i$ since the near-field effects are dominant. Bethe and Bouwkamp [54, 55] have shown the exact analytical solution for the transmission from subwavelength circular apertures on an infinitely thin metal film with infinite conductivity. The aperture is theoretically treated as a magnetic dipole located in the plane of hole. The transmission coefficient is calculated to be proportional to $\left(\frac{r}{\lambda_i}\right)^4$ which is a very small value and agrees with the Rayleigh's theory of scattering by small objects.

For a metal film with finite thickness Bethe and Bouwkamp's model is applicable for apertures which allow only decaying modes. This condition is satisfied for the cases where the diameter of the aperture is related to the initial wavelength by $d \leq 0.3\lambda_i$ for circular and $d \leq \frac{\lambda_i}{2}$ for square holes [9]. For the cases where the propagating modes are allowed, this theory is not applicable and the transmission observed is higher owing to the waveguide behavior.

A real metal film has a finite thickness and a finite conductivity therefore it is not perfectly opaque which renders the theory of Bethe and Bouwkamp invalid. A metal film is opaque for thickness on the order of several skin depths. That kind of apertures prevents the tunneling of the radiation and therefore the localized surface plasmons play a significant role in the transmission phenomenon [56].

The transmission of incident light on a metal film with a periodic array of subwavelength apertures can be enhanced due to the excitation of SPPs via grating coupling. The SPP field energy is then tunneled to the other side of the metal and scattered into the far field on the other side. Ebbesen et. al. observed an extraordinary transmission of light through the surface of a thin metal film with a subwavelength hole array where the transmission coefficient is larger than unity ($T > 1$). The light that tunnels through the aperture was more than the incident light on the area of the aperture. The peaks of the transmitted light occur at the wavelengths which allow the excitation of the SPPs by the grating structure showing clearly that the transmission phenomena is mediated by propagating SPPs through the apertures.

Observation of the extraordinary transmission is also possible for single apertures surrounded by grating-like surface corrugations/grooves where the incident light is coupled to the propagating SPPs by grating coupling and transmitted through the slit [57, 58]. Also a bull's eye structure where concentric circular grooves surround a single subwavelength hole and act as a grating structure leads to the observation of the transmission that is higher than unity ($T > 1$) at the wavelengths that SPPs are excited [59].

The effect of the geometrical parameters on the transmission is studied by many groups in ref. [60-64] which confirmed the SPPs have an important role in the transmission process.

In a one dimensional slit structure where the slit allows the propagation of the SPPs transmission is due to the resonances of the slit waveguide mode and depends on the thickness of the metal film [65, 66].

The transmission through a single aperture involves the excitation of localized surface plasmon (LSP) modes at the edges of the aperture. Single aperture diameter is effectively increased when the localized surface plasmons are excited.

The transmission is enhanced due to this increase since the cut off wavelength of the fundamental waveguide mode is increased [67].

For a single subwavelength aperture, the dimensions of the aperture can be optimized for maximum transmission. The geometrical from of the aperture determines the spectral position of the LSP mode. The transmission increases due to the field enhancement at the rim of the aperture at the wavelength which allows the LSP excitation [56].

The field transmission through a single subwavelength aperture can be enhanced by several methods that will improve the coupling between the interfaces of incidence and exit. Using multilayer structures [68, 69] or filling the aperture with a high index dielectric [70] can be listed as some of these methods.

4.2. Applications of extraordinary transmission and SP interferometry

Extraordinary transmission through subwavelength apertures on metal films that is first observed by Ebbesen started a new research subject which is based on understanding of fundamentals of nano-optics. This intriguing property also led to practical applications in experimental studies. In this section some of the important applications of this transmission phenomenon and studies and sensors based on surface plasmon interferometry will be reviewed.

A fundamental observation from Young's double slit experiment has been applied to surface plasmons by Schouten et al. [47]. The transmission from two parallel subwavelength slits which are separated by many optical wavelengths is studied. Far field double slit pattern is observed that can be enhanced or reduced by modifying the wavelength of the incident light. The angle integrated transmission coefficient is studied and the polarization dependence and the wavelength dependent nature of the transmission showed that the surface plasmon assistance exists. Figure 4.1 (a) shows the schematic of the experiment.

Enhanced transmission is used in applications such as enhancement of fluorescent emission from molecules that are placed in a subwavelength aperture by Rigneault et al. [53] and further developed by adding circular grooves around the aperture and creating bull's eye structure [71] explained in the previous section.

Sensor applications of the extraordinary transmission phenomenon are also studied widely where the applications are based on nanohole array surface plasmon resonance sensing [3, 4, 51, 52, 72] or surface plasmon interferometry.

In the previous section the wavelength dependence of the surface plasmon resonance at the nanohole arrays was explained. This wavelength dependence allows the usage of nanohole arrays as refractive index sensors since the resonance wavelength shifts by changing refractive index of the medium surrounding the nanohole arrays [51, 72]. Lee et al. also showed that quasi one-dimensional nanoslit arrays also can be used for refractive index sensing. It has a sensitivity comparable to that of two dimensional nanohole arrays [52]. Refractive index sensitivity studies also led to the use of nanohole arrays for detection of the adhesion of self assembled monolayers and the adhesion of proteins and binding of organic molecules to the metallic surface [4]

Surface plasmon interferometry is based on the interference of surface plasmon polaritons excited by a pair of subwavelength slits or a slit-groove pair. There are many studies on surface plasmon interferometry which are based on the measurement of the transmission spectrum [5, 47, 48]. In 2007, Temnov and Woggon [48] have used surface plasmon interferometry to measure the group velocity of surface plasmons propagating on a thin metal film on which a groove and a slit is etched by focused ion beam (FIB). They have measured surface-plasmon-mediated interference in the spectral domain. In Fig 4.1 (b) their experimental geometry is shown. Imaging spectrometer is used to record the transmission of the white light that illuminates the slit. The transmission spectra that they observed shows wavelength dependent oscillations that agree with the work conducted by Schouten et al. [47]. The oscillations indicate that the SPPs

that are excited at the slit propagate through the groove and the partially scattered SPPs from the groove propagate back to the slit and interfere with the directly transmitted light from the slit. The SPP scattering from rectangular grooves are studied in detail by Kuttge et al. [19] and Brucoli and Martín-Moreno [18] as depicted in the chapter two. The study of the transmission oscillations leads the calculation of the group velocity of the SPPs in agreement with the theoretical values.

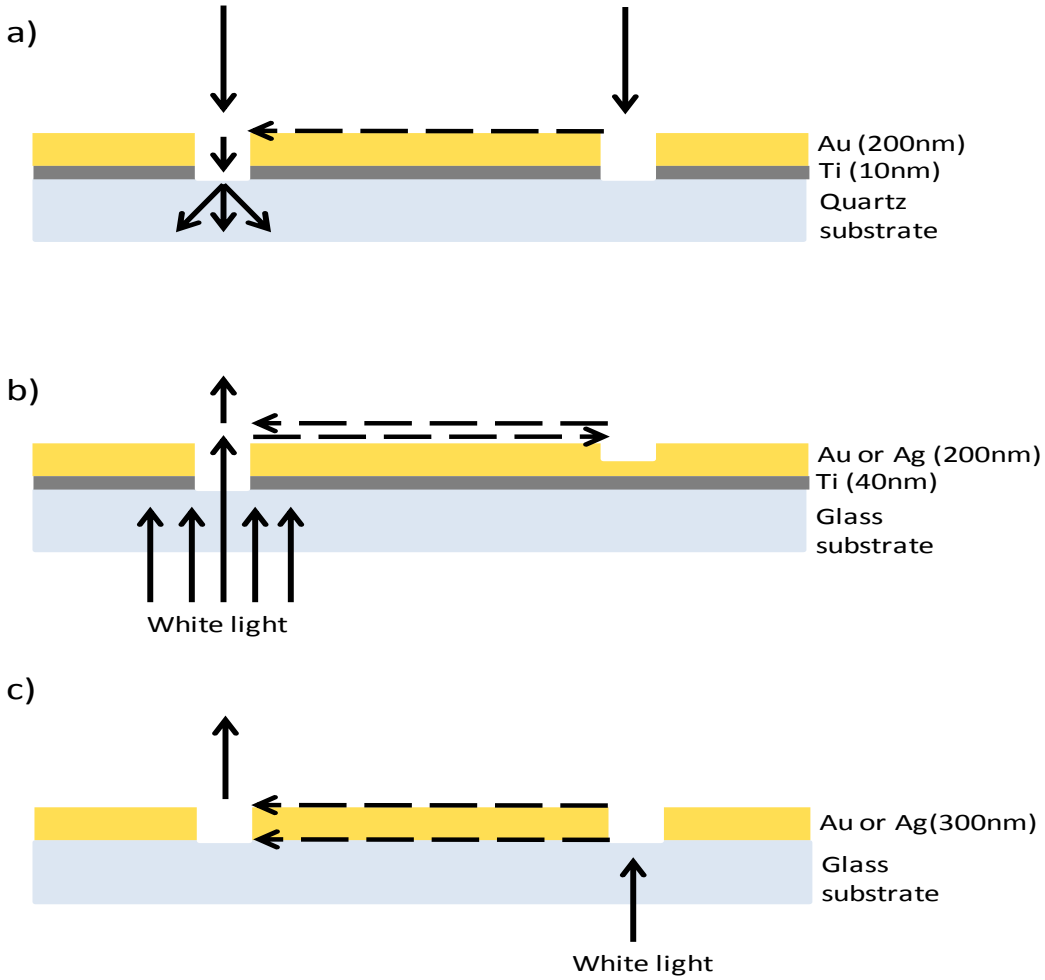

Figure 4.1 (a) Schematic of the plasmon assisted double slit experiment conducted by Schouten et al. [47] a few nm of Ti layer is coated as adhesion layer and thin film is coated on it. There are two parallel slits etched on the Au thin film. When illuminated from above the SPPs generated at the slit on the right propagates and interferes with the transmitting light on the left and vice versa. The surface plasmon is then back converted into free space radiation. The propagating SPPs are indicated by the dashed line. (b) Schematic of surface plasmon interferometer used by Temnov et al [48] to measure the group velocity of surface plasmons. (c) Vertical Plasmonic Mach Zehnder Interferometer [6]

Interferometry is a very sensitive method that is used to measure and study the binding of molecules on the surface and interactions between molecules. Therefore recently surface plasmon interferometry studies have attracted attention as a sensing method of changes in the index of refraction [5-7]. Debackere et al. [7] have used the excitation of SPPs by waveguide where the plasmon modes at the upper and lower interface of the metal layer have different phase. The

interference of these two modes was observed in the output waveguide. Any change in the bulk refractive index of the dielectric above the metal layer resulted in the change of the interference. The shift in the transmission spectra as the refractive index changes was also presented.

Vertical plasmonic Mach-Zehnder Interferometer (VPMZI) was used for sensitive optical sensing in 2009 by Gan et al. [6] where two parallel nanoslits were perforated on a metal film that is on a glass substrate. Figure 4.1 (c) shows the interference scheme of the VPMZI. Both sides are available to support SPP propagation and the interference generated by these SPPs is used to sense the refractive index changes on the metal surface.

The most recent plasmonic interferometer for biosensing is presented by Feng et al. [5] where parallel groove slit groove (GSG) configurations integrated with microfluidics are used with varying slit groove distances (Figure 4.2). It is a multispectral interferometer where the GSG configuration is illuminated by a multi-wavelength light and the interference of the two surface plasmon modes generated at the grooves are interfered at the slit with the directly transmitted light through the slit. The spectral transmission through the slit is interrogated. The transmitted intensity depends on the wavelength and the distances between the grooves and the slit. The presented sensor has 20fL of sensing volume and resolution of $\sim 3 \times 10^{-7}$RIU (refractive index unit).

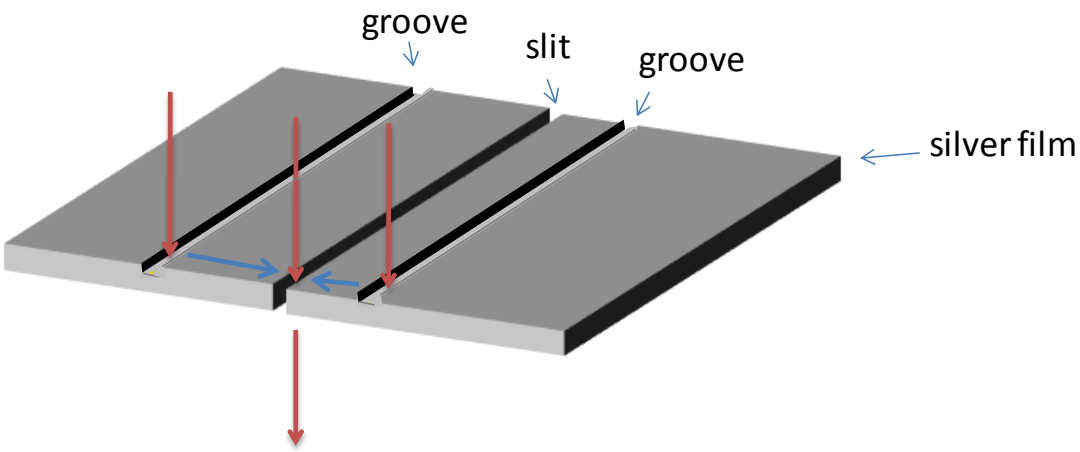

Figure 4.2 Schematic of parallel groove-slit-groove (GSG) configurations from the plasmonic interferometer presented by Feng et al. [5]. The slit-groove separation distances vary between 0.2 and 10 μm. When the surface is illuminated, the SPPs generated at the gro grooves (blue) propagate towards the slit and interferes with each other and directly transmitted light through the slit and at the other side of the slit it is converted into free space radiation (below).

The works that are reviewed in this chapter illustrates the importance and the prevalence of the surface plasmon resonance sensors that derive the benefit from plasmonic interferometry. All of the presented sensors use the analysis of the transmission spectra of the multifrequency light. In this thesis we present a plasmonic interferometer for high-throughput sensing which does not require any spectral measurement and provides more practical sensing scheme by interference pattern interrogation.

Chapter 5

Subwavelength Plasmon Interferometer for High-Throughput Sensing

This chapter will be published in Optics Letter as “Subwavelength plasmon interferometer for high-throughput sensing” Ozlem Yavas, Coskun Kocabas, Vol 37, Iss. 16, pp. 3396-3398. Reproduced (or ‘Reproduced in part’) with permission from Optical Society of America.

Small detection volume [73], increased analysis speed and reduced cost [74] are the main driving forces for miniaturized lab-on-a-chip systems [75]. Subwavelength holes on opaque metal films provide a unique configuration for miniaturized sensors. Transmitted light through these tiny holes is governed by the electronic resonance in the surface of the metal film. Excitation of surface plasmon-polaritons (SPPs) on the metal-dielectric interface characterizes the resonance condition. The sensitive dependence of the plasmon resonance condition on the dielectric constant of the medium is used for label free sensing applications [76].

Surface plasmon resonance sensors (SPR) are widely used to measure biomolecular interactions on functionalized metal surfaces [8, 77, 78]. SPPs are confined electromagnetic modes at an interface between two media with opposite permittivity at the working wavelength, i.e. metal-dielectric interface. Gold, silver

and aluminum has negative dielectric constants at the visible spectrum, therefore they are used as a metal substrates to support SPPs. Variation of the dielectric constant of the medium on the metal layer changes the wavevector of SPPs, results in a change in the excitation efficiency. Detecting the reflected power from the metal surface through a prism provides a sensitive means of detecting index of refraction. Surface specific detection together with the high sensitivity allows the widespread acceptance of SPR sensors. Different types of SPR sensors have been proposed to increase the detection sensitivity [79, 80]. Sensing schemes based on long-range SPs [43], localized SPs [81] and transmission through nanohole arrays are examples for sensitive ones. Signal interrogation techniques give another degree of freedom to optimize SPR sensors. Various physical parameters, such as intensity, wavelength [82] and phase [83], have been implemented with different interferometer geometries to improve the detection sensitivity. Recently, subwavelength plasmon interferometers [84, 85] received attention due to their small detection volume and large sensitivity. Different combinations of parallel grooves and slits generate spectral interference in the transmitted light [86]. Measuring the spectrum of the transmitted light provides sensitive methods for label free sensing [5]. Due to the requirement of a tunable light source or a spectrometer, multispectral plasmon sensors are not very practical for high throughput applications.

In this Thesis, we demonstrate a refractive index sensor based on a subwavelength plasmon interferometer using monochromatic light. Very high contrast fringe pattern is generated by the plasmon interferometer that consists of a sub-wavelength slit-groove pair with a small angle between them. The small angle between the groove and the slit provides spatially varying slit-groove distance which generates a high-contrast interference pattern. By interrogating the relative position of interference fringes, one can determine the refractive index of the dielectric medium on the metal surface. This is a practical yet very sensitive refractive index measurement scheme. The developed subwavelength plasmon interferometer has four distinct advantages: (1) the interferometer uses

monochromatic light, (2) the sensor does not need a bulky prism or grating structures to excite SPPs, (3) the signal interrogation requires a simple image processing, and (4) the sensor has very small detection volume (100fL).

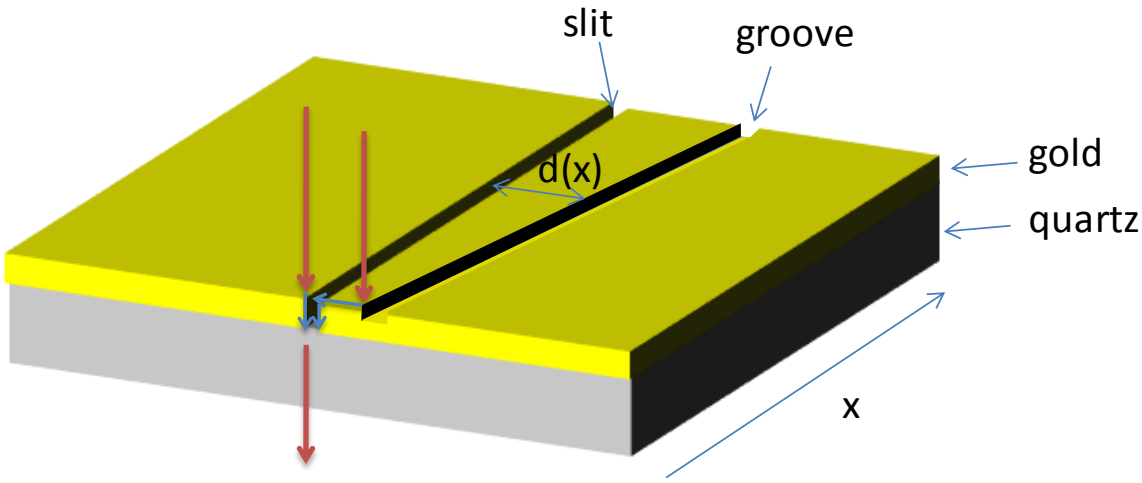

Figure 5.1 Schematic representation of the plasmon interferometer. The interferometer is fabricated on a quartz substrate coated with 150nm thick gold film.

Figure 5.1 shows the schematic drawing of the plasmon interferometer. The interferometer consists of a sub-wavelength slit-groove pair with a small angle between them. The distance between the slit and the groove varies with the position x along the slit, as $d(x) = x \sin\theta$ where θ is the tilt angle. Similar structures were fabricated with the tilt angle (θ) of 5^0, 10^0 or 15^0. Scanning electron microscope (SEM) images of the fabricated slit-groove pairs with tilt angles of 5, 10 and 15 degrees are given in Fig. 5.2a,b and c respectively.

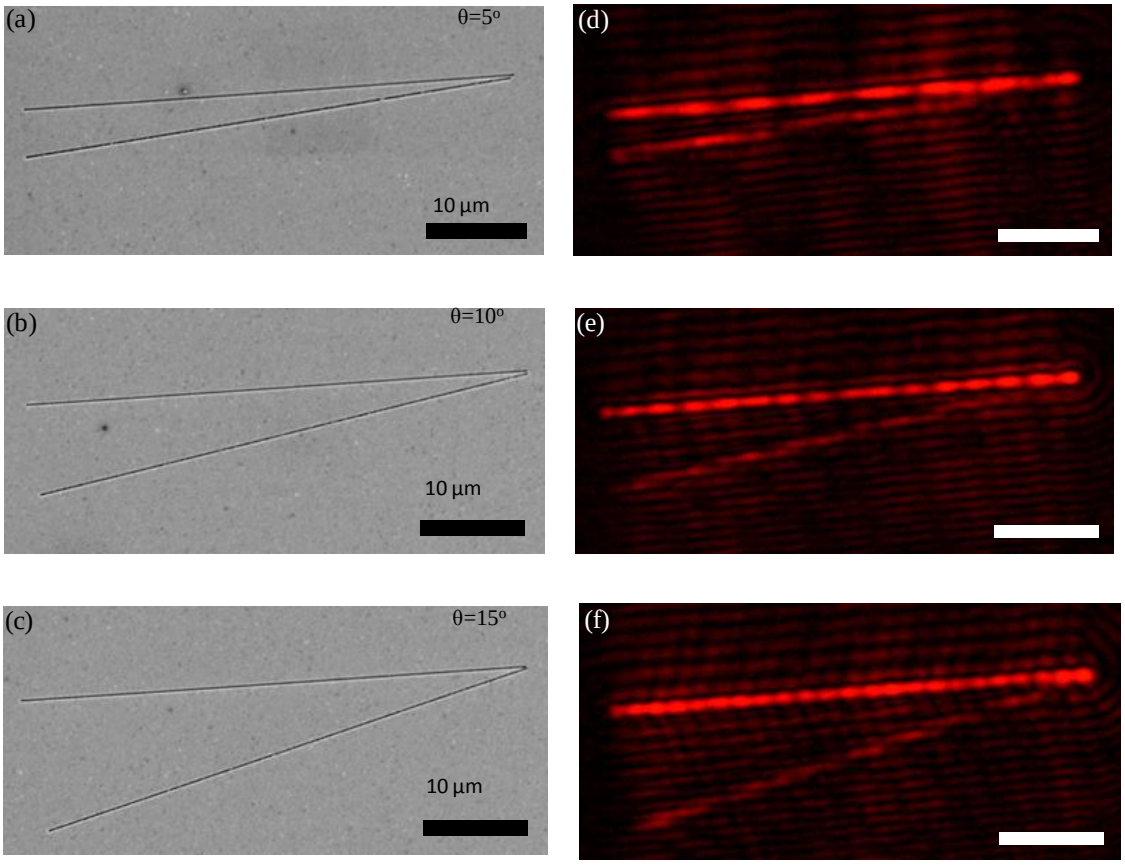

Figure 5.2 (a,b,c) Scanning electron microscope images of the fabricated plasmon interferometer with grove-slit angle of 5, 10 and 15 degrees, respectively. The width of groove and slit is 200nm and 100 nm. (d,e,f) Optical microscope images of the interference fringe pattern generated by the interference of SPPs excited by the groove and the slit pair when the surface is illuminated by a diode laser with wavelength of 635nm. The scale bars are 10 μm.

The slit-groove pairs are etched using focused Ga^+ ions with 50pA on 150 nm thick gold film deposited on a quartz substrate. We observed that to obtain high contrast fringes, the metal film should be thicker than 100 nm. The length of the slit and groove are 50μm. The width of the slit and the groove is 100 nm and 200 nm, respectively. The slit extends through the gold layer, and the groove has a depth of 100 nm.

To obtain the interference patterns, we illuminated the slit-groove pairs with a collimated diode laser (λ=635 nm). The polarization of the laser is orthogonal to the slit length. The transmitted light was imaged by a CCD camera (Scion Corp.) through a microscope objective. The optical micrographs of high contrast fringe patterns due to the interference of SPPs are shown in Fig. 5.2d,e and f, for groove-slit angle of 5, 10 and 15 degrees, respectively. In contrast to the multispectral plasmon interferometers reviewed in the previous chapter, the tilt angle allows us to obtain the interference pattern with monochromatic light. The SPPs interfere as they propagate through the slit. The plasmons generated by the groove accumulate a phase as they propagate the separation distance between the groove and slit. Since the separation distance varies along the slit, a sinusoidal interference pattern is observed. The period of the interference pattern (Λ) can be written as

$$\Lambda = \lambda / n_{eff} \sin\theta \tag{5.1}$$

where λ is the wavelength of the light source, n_{eff} is the effective index of SPPs and θ is the tilt angle. The effective index can be written as

$$n_{eff} = [\varepsilon_d \varepsilon_m / (\varepsilon_d + \varepsilon_m)]^{1/2} \tag{5.2}$$

where ε_m and ε_d are the dielectric constant of the metal and dielectric, respectively. The period for tilt angles of 5, 10 and 15 degrees calculated for gold-water interface are 5.08, 2.55, 1.71μm, respectively.

To test the performance of the sensor, we integrated the plasmon interferometer with a microfluidic device. The microfluidic device was fabricated using PDMS (polydimethylsiloxane) based rapid prototyping [87]. The medium flowing inside the microchannel is deionized water and the refractive index is controlled by varying the concentration of salt (*NaCl*). The interference pattern is imaged by a CCD camera. Fig 5.3 shows the configuration of the experimental setup and Figure 5.4 shows the CCD images taken with no fluid flowing through the channel (Fig. 5.4a) and with water flowing through the channel (Fig. 5.4b). The refractive index change is so high that the number of fringes has changed. Figure 5.4c and d shows the Matlab simulations of the two cases shown in Fig 5.4a and b. The theoretical plots of the intensity profiles are generated by Matlab with the method and parameters that will be described below and they agree with the intensity profiles of the CCD images.

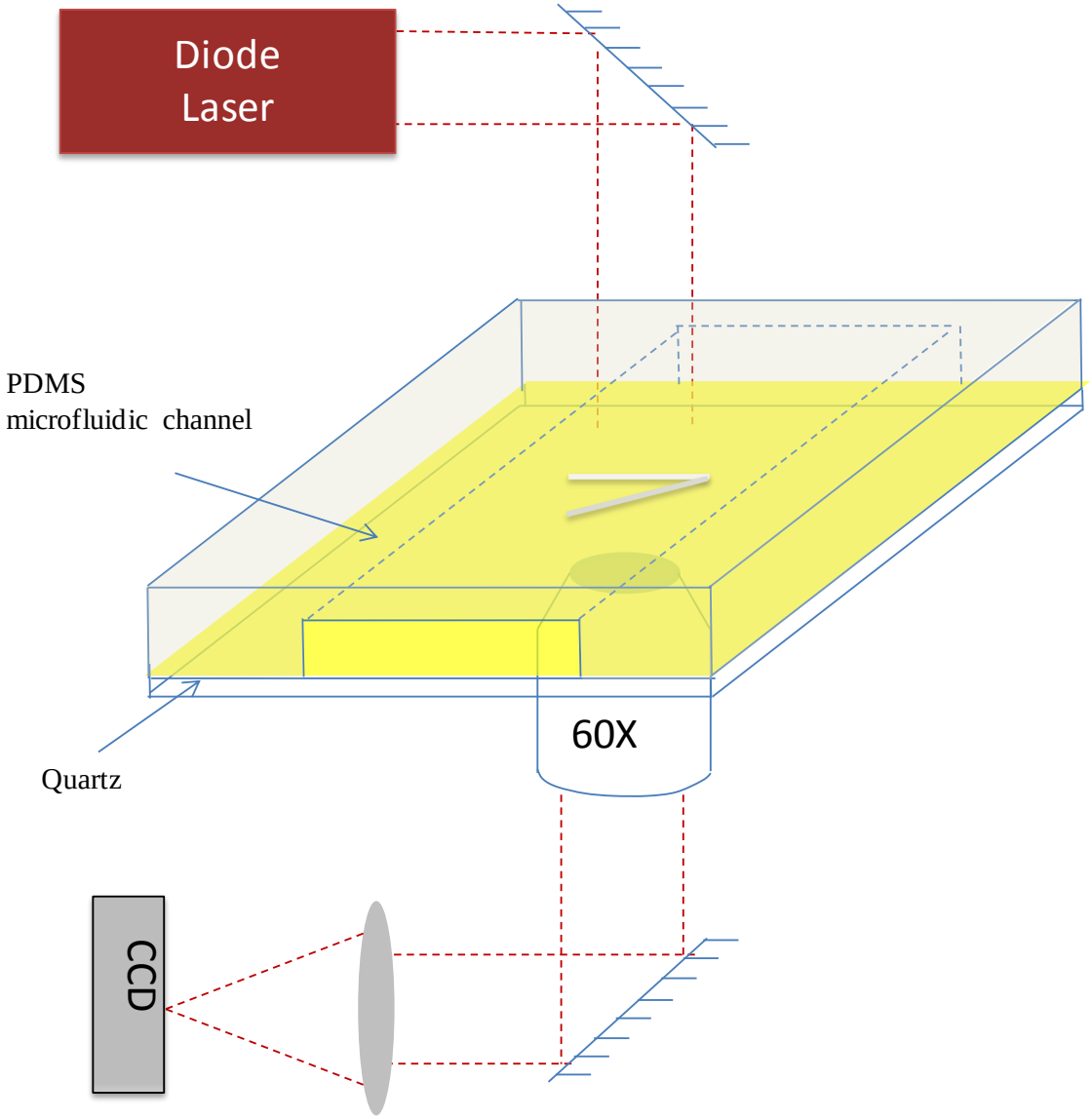

Figure 5.3 The experimental setup to test the sensitivity of the sensor.

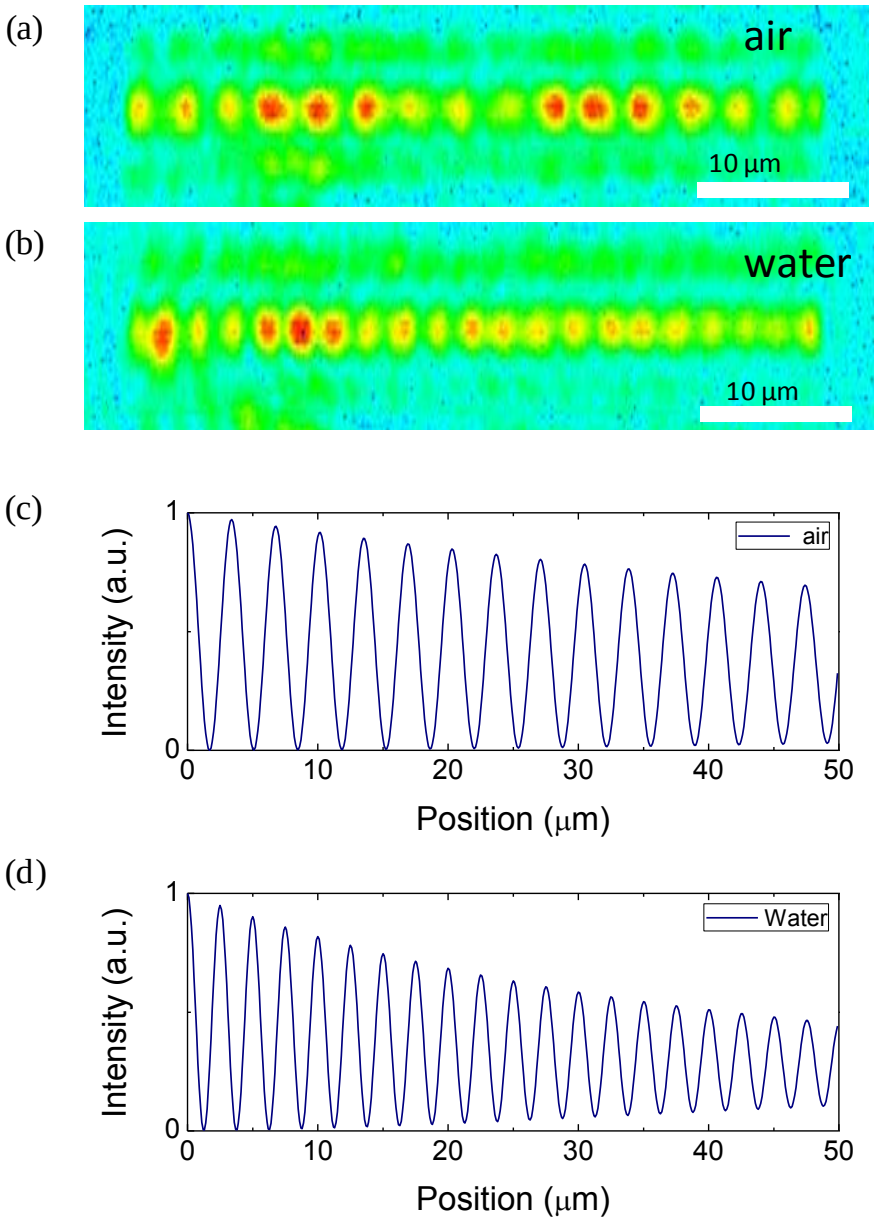

Figure 5.4 (a,b) CCD images taken by illuminating the slit groove pair with tilting angle of 10 degrees with air-gold interface (a) and with water-gold interface (b). (c,d) The Matlab simulations of the intensity profile along the slit for air-gold (c) and water- gold interfaces.

Fig. 5.5a shows overlaid images of interference pattern obtained for various index of refraction between 1.34 to 1.37. There are 21 fringes in the length of 50 μm. We indexed the fringes starting from the intersection point of the groove and the slit. When we increased refractive index of the liquid, we observed that the period of the interference pattern decreases and the fringes shift spatially toward the intersection point. To guide the eye, we drew lines connecting the center of fringes in Fig. 5.5a. The displacement of the fringes depends the total accumulated phase as SPPs move from the groove to the slit. This phase is a function of wavevector of SPP and the groove-slit separation distance as

$$\Delta\Phi(x) = k'_{spp}\, d(x) \tag{5.3}$$

The fringe displacement increases linearly with the fringe number. The position of the first fringe (at the intersection point) stays constant owing to the small groove-slit separation distance. We measured the relative position of the fringes with respect to the first one. Fig. 5.5b shows the intensity distribution of the first three fringes. Fig. 5.5c shows the last four fringes on the interferometer. The fringe displacement increases linearly with the groove-slit separation distance. Fig. 5.5d shows the fringe displacement for 1st, 14th and 20th fringes as function of index of refraction.

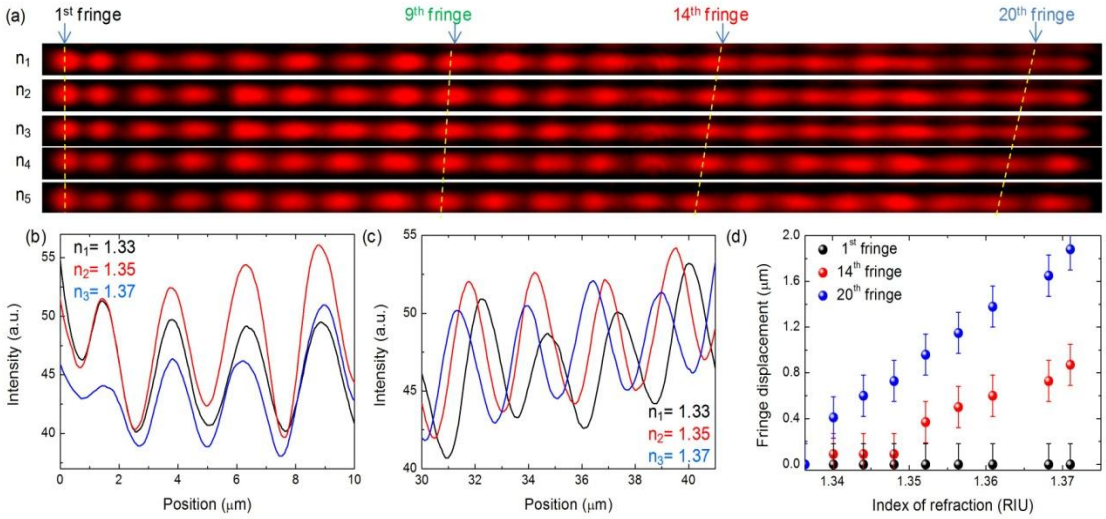

Figure 5.5 (a) Optical microscope images of the fringe pattern generated by plasmon interferometer with a tilting angle of 10 degrees, integrated in a microfluidic device. The index of refraction of the medium is varied linearly between n_1=1.34 and n_5=1.37. The pattern has 21 fringes. The relative position of the fringes shifts as the index of refraction changes. (b,c) Spatial intensity distribution of the first and last four fringes. The relative positions of first fringes stay nearly constant. (d) Fringe displacement as a function of index of refraction. The slope of the curve provides the sensitivity of the sensor.

To understand the ultimate performance of the demonstrated plasmon interferometer, we would like to develop a numerical model to calculate the interference pattern and the detection sensitivity. As the surface is illuminated by collimated light, both groove and slit generates SPPs on the metal surface. The SPPs generated by the slit are transmitted through the metal, whereas the SPPs generated by the groove travels the slit-groove separation distance, *d(x)*, and then they are transmitted to the other side of the metal. The presence of two phase-shifted electric fields at the slit position produces interference. The intensity of the transmitted light is square of the total electric field intensity at the slit.

Total intensity of the transmitted light through the slit is written as [48, 88]

$$I(x) = E_1(x)^2 + E_2(x)^2 + 2E_1E_2\cos(\Phi(x)) \tag{5.4}$$

where $E_1(\mathrm{x})$ and $E_2(\mathrm{x}) \propto \mathrm{e}^{-k''_{spp}\,\mathrm{d(x)}}$ are the intensities of the transmitted light generated by slit and groove, respectively. The phase difference between the two electric field is

$$\Phi(x) = k'_{spp}d(x) + \Phi_0 \tag{5.5}$$

where k'_{spp} and k''_{spp} are the real and imaginary part of the surface plasmon wavevector $k_{spp} = k'_{spp} + ik''_{spp}$. Φ_0 is unknown constant phase shift that arises from the differences of the propagated distance in air and the coupling of surface plasmons at the groove and the slit. The imaginary part of the wavevector defines the optical loss on the metal film. Figure 5.6a shows the calculated normalized intensity distribution along the interferometer with a slit-groove angle of 10 degrees. The inset in Fig. 5.6a shows the recorded CCD image of the interference pattern. There is a very good agreement between the observed and calculated fringe pattern. The contrast of the fringes decreases with increasing fringe number because of the optical loss of the metal. The period of the fringe pattern decreases with increasing index of refraction ($\Lambda = \lambda/n_{eff}\sin\theta$). Figure 5.6b shows the

calculated (blue line) and measured (scattered plot) period of the fringe pattern. An easy way to find the refractive index of the medium is to record the relative displacement of the fringes. Fig. 5.6c shows the displacement of the fringes normalized by the period of the fringe pattern (Λ) as a function of change of index of refraction. The normalized displacement increases linearly with the fringe index. To quantify the sensitivity we define two types of figure of merit; normalized displacement per refractive index,

$$S1 = \Delta x / \Lambda \Delta n \tag{5.6}$$

and normalized intensity change per refractive index unit,

$$S2 = \Delta I / I \Delta n \tag{5.7}$$

The inset in Fig. 5.6c shows the calculated displacement sensitivity S1 as a function of fringe index. Displacement sensitivity, S1, of 17 RIU^{-1} can be obtained with the 21th fringe of a plasmon interferometer with a length of 50 μm. The calculated normalized intensity change per refractive index unit, S2, is shown in Figure 5.6d as function of position along the slit. The sensitivity increases along the slit and reaches to a maximum value of 70 RIU^{-1} around 50 μm. For longer slit-groove distances sensitivity starts to decrease owing to the optical loss of the metal surface.

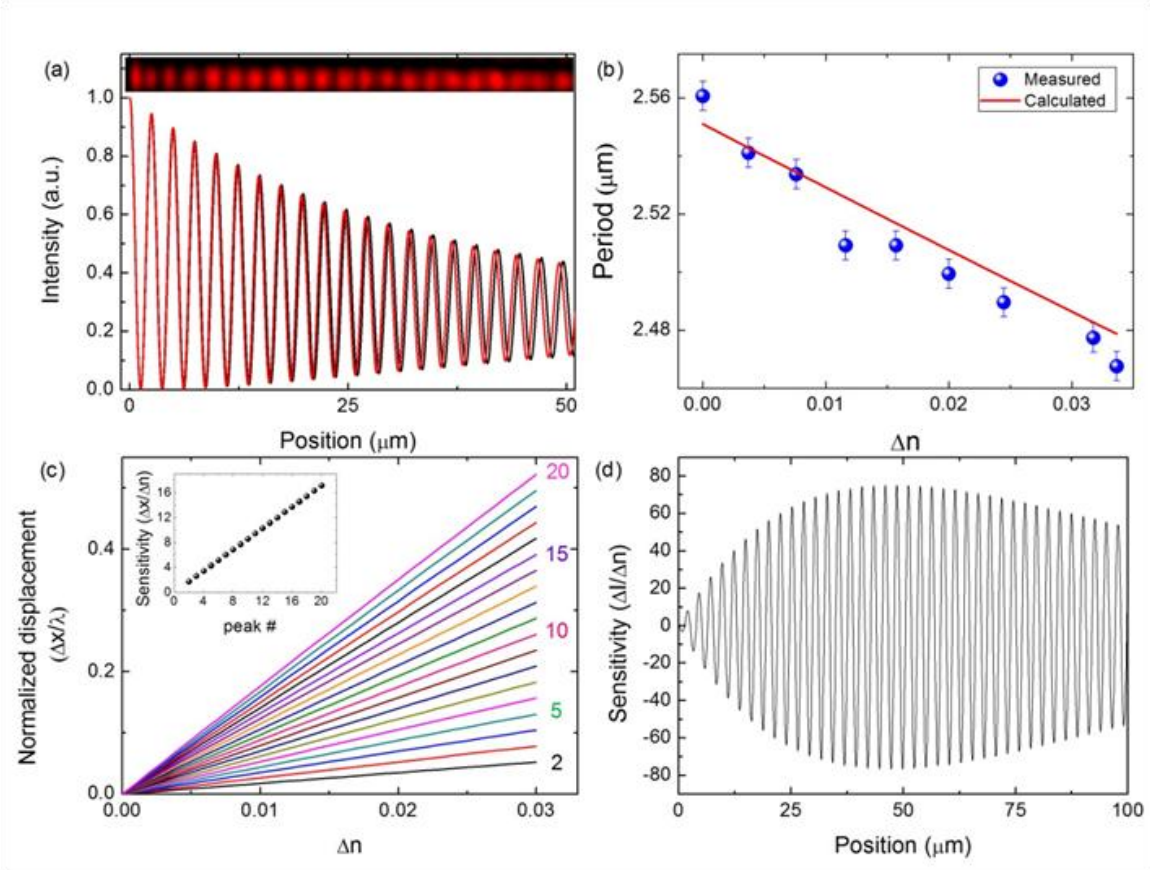

Figure 5.6 (a) Calculated interference fringes for two different index of refraction (n=1.33, black curve, n=1.34, red curve) generated by a plasmon interferometer with a length of 50 μm and a slit-groove angle of 10 deg. The inset shows the CCD image of the interference fringes. (b) Measured and calculated period of the fringe pattern as a function of change of index of refraction. (c) Normalized displacement of the fringes as a function of change of index of refraction. The inset shows the sensitivity as a function of fringe index. (d) Normalized intensity change along the slit position.

Chapter 6

Conclusion

In this thesis we demonstrated a sensitive sensor based on a sub-wavelength plasmon interferometer. The small size of the sensor together with the ability to be integrated with microfluidic devices are the advantages of the presented sensor. Oblique orientation of the slit-groove pair introduces a position dependent phase difference which generates repeating constructive and destructive fringes along the interferometer. Interrogation of the position and the intensity of the fringes provide sensitive means for refractive index measurements. This sensor, unlike the previous plasmon interferometry based sensors, provides a very practical scheme which does not require spectral analysis of the transmitted light through the slit. The fringe pattern interrogation is a simple image processing method. This practical scheme can also be improved by using different geometries of slit groove pairs or nanohole and circular groove pairs. The fringe contrast can also be improved by using mirror symmetric grooves at the both sides of the slit. If these grooves have the same angle and distance from the slit, the position dependent phase shift would be same at the both sides, leading higher contrast fringes.

Different fabrication methods can be used to eliminate the difficulty of using focused ion beam (FIB). As an example the phase shift lithography is a practical lithography method for generating slits. The groove generation may need more steps of lithography techniques. Still the cost may be reduced by using lithography techniques.

We have tested our interferometer to detect the refractive index variations on the surface as presented. The sensor can further be used for label free analysis of molecular binding on metal surface or molecular interactions in bulk solutions.

Bibliography

1. Girlando, A., et al., *Raman-Spectra of Molecules on Metal-Surfaces.* Surface Science, 1980. **101**(1-3): p. 417-424.
2. Ebbesen, T.W., et al., *Extraordinary optical transmission through sub-wavelength hole arrays.* Nature, 1998. **391**(6668): p. 667-669.
3. Gordon, R., et al., *Plasmonic sensors based on nano-holes: Technology and integration - art. no. 695913.* Micro (Mems) and Nanotechnologies for Space, Defense, and Security Ii, 2008. **6959**: p. 95913-95913.
4. Brolo, A.G., et al., *Surface plasmon sensor based on the enhanced light transmission through arrays of nanoholes in gold films.* Langmuir, 2004. **20**(12): p. 4813-4815.
5. Feng, J., et al., *Nanoscale Plasmonic Interferometers for Multispectral, High-Throughput Biochemical Sensing.* Nano Letters, 2012. **12**(2): p. 602-609.
6. Gan, Q.Q., Y.K. Gao, and F.J. Bartoli, *Vertical Plasmonic Mach-Zehnder interferometer for sensitive optical sensing.* Optics Express, 2009. **17**(23): p. 20747-20755.
7. Debackere, P., R. Baets, and P. Bienstman, *Bulk sensing experiments using a surface-plasmon interferometer.* Optics Letters, 2009. **34**(18): p. 2858-2860.
8. Kabashin, A.V. and P.I. Nikitin, *Surface plasmon resonance interferometer for bio- and chemical-sensors.* Optics Communications, 1998. **150**(1-6): p. 5-8.
9. Maier, S.A., *Plasmonics : fundamentals and applications*. 1st ed. 2007, New York: Springer. xxiv, 223 p.
10. Fox, M., *Optical properties of solids*. 2001, Oxford ; New York: Oxford University Press. xii, 305 p.
11. Kretschmann, E.a.H.R., *Radiative decay of non-radiative surface plasmon excited by light.* Z. Naturforsch, 1968. **23A**: p. 2135-2136.
12. Otto, A., *Excitation of surface plasma waves in silver by the method of frustrated total reflection.* Z Physik, 1968. **216**: p. 398-410.
13. Homola, J.r. and J. Dostálek, *Surface plasmon resonance based sensors*. Springer series on chemical sensors and biosensors,. 2010, Berlin ; New York: Springer. xii, 251 p.
14. Verhagen, E., L. Kuipers, and A. Polman, *Field enhancement in metallic subwavelength aperture arrays probed by erbium upconversion luminescence.* Optics Express, 2009. **17**(17): p. 14586-14598.
15. Chremmos, I., *Magnetic field integral equation analysis of surface plasmon scattering by rectangular dielectric channel discontinuities.* Journal of the Optical Society of America a-Optics Image Science and Vision, 2010. **27**(1): p. 85-94.

16. Leveque, G., O.J.F. Martin, and J. Weiner, *Transient behavior of surface plasmon polaritons scattered at a subwavelength groove.* Physical Review B, 2007. **76**(15).
17. Satuby, Y. and M. Orenstein, *Surface-Plasmon-Polariton modes in deep metallic trenches- measurement and analysis.* Optics Express, 2007. **15**(7): p. 4247-4252.
18. Brucoli, G. and L. Martin-Moreno, *Effect of defect depth on surface plasmon scattering by subwavelength surface defects.* Physical Review B, 2011. **83**(7).
19. Kuttge, M., F.J.G. de Abajo, and A. Polman, *How grooves reflect and confine surface plasmon polaritons.* Optics Express, 2009. **17**(12): p. 10385-10392.
20. Fisher, R.D., et al., *Structure and ubiquitin binding of the ubiquitin-interacting motif.* Journal of Biological Chemistry, 2003. **278**(31): p. 28976-28984.
21. Herminjard, S., et al., *Surface Plasmon Resonance sensor showing enhanced sensitivity for CO2 detection in the mid-infrared range.* Optics Express, 2009. **17**(1): p. 293-303.
22. Hotta, K., A. Yamaguchi, and N. Teramae, *Properties of A Metal Clad Waveguide Sensor Based on A Nanoporous-Metal-Oxide/Metal Multilayer Film.* Analytical Chemistry, 2010. **82**(14): p. 6066-6073.
23. McDonnell, J.M., *Surface plasmon resonance: towards an understanding of the mechanisms of biological molecular recognition.* Current Opinion in Chemical Biology, 2001. **5**(5): p. 572-577.
24. Huang, Y., et al. *Research on Surface Plasmon Resonance Sensor Based on Wavelength Modulation by Using Theoretical Simulation Resonance Sensor Based on Wavelength Modulation by Using Theoretical Simulation*. in *Measuring Technology and Mechatronics Automation (ICMTMA), 2011 Third International Conference on*.
25. Oshannessy, D.J., et al., *Determination of Rate and Equilibrium Binding Constants for Macromolecular Interactions Using Surface-Plasmon Resonance - Use of Nonlinear Least-Squares Analysis-Methods.* Analytical Biochemistry, 1993. **212**(2): p. 457-468.
26. Zacher, T. and E. Wischerhoff, *Real-time two-wavelength surface plasmon resonance as a tool for the vertical resolution of binding processes in biosensing hydrogels.* Langmuir, 2002. **18**(5): p. 1748-1759.
27. Regatos, D., et al., *Au/Fe/Au multilayer transducers for magneto-optic surface plasmon resonance sensing.* Journal of Applied Physics, 2010. **108**(5).
28. Nylander, C., B. Liedberg, and T. Lind, *Gas-Detection by Means of Surface-Plasmon Resonance.* Sensors and Actuators, 1982. **3**(1): p. 79-88.
29. Ma, X., et al., *Dynamically modulated intensity interrogation scheme using waveguide coupled surface plasmon resonance sensors.* Sensors and Actuators a-Physical, 2010. **157**(1): p. 9-14.
30. Liedberg, B., C. Nylander, and I. Lundstrom, *Surface-Plasmon Resonance for Gas-Detection and Biosensing.* Sensors and Actuators, 1983. **4**(2): p. 299-304.
31. Li, C.T., T.J. Yen, and H.F. Chen, *A generalized model of maximizing the sensitivity in intensity-interrogation surface plasmon resonance biosensors.* Optics Express, 2009. **17**(23): p. 20771-20776.
32. Rich, R.L. and D.G. Myszka, *Survey of the year 2003 commercial optical biosensor literature.* Journal of Molecular Recognition, 2005. **18**(1): p. 1-39.

33. Rich, R.L. and D.G. Myszka, *Survey of the year 2004 commercial optical biosensor literature.* Journal of Molecular Recognition, 2005. **18**(6): p. 431-478.
34. Jorgenson, R.C. and S.S. Yee, *A Fiberoptic Chemical Sensor-Based on Surface-Plasmon Resonance.* Sensors and Actuators B-Chemical, 1993. **12**(3): p. 213-220.
35. Zhang, L.M. and D. Uttamchandani, *Optical Chemical Sensing Employing Surface-Plasmon Resonance.* Electronics Letters, 1988. **24**(23): p. 1469-1470.
36. Sepulveda, B., et al., *Highly sensitive detection of biomolecules with the magneto-optic surface-plasmon-resonance sensor.* Optics Letters, 2006. **31**(8): p. 1085-1087.
37. Sjolander, S. and C. Urbaniczky, *Integrated Fluid Handling-System for Biomolecular Interaction Analysis.* Analytical Chemistry, 1991. **63**(20): p. 2338-2345.
38. Lofas, S., et al., *Bioanalysis with Surface-Plasmon Resonance.* Sensors and Actuators B-Chemical, 1991. **5**(1-4): p. 79-84.
39. Liedberg, B., I. Lundstrom, and E. Stenberg, *Principles of Biosensing with an Extended Coupling Matrix and Surface-Plasmon Resonance.* Sensors and Actuators B-Chemical, 1993. **11**(1-3): p. 63-72.
40. Wu, S.Y., et al., *Highly sensitive differential phase-sensitive surface plasmon resonance biosensor based on the Mach-Zehnder configuration.* Optics Letters, 2004. **29**(20): p. 2378-2380.
41. Dostalek, J., J. Homola, and M. Miler, *Rich information format surface plasmon resonance biosensor based on array of diffraction gratings.* Sensors and Actuators B-Chemical, 2005. **107**(1): p. 154-161.
42. Telezhnikova, O. and J. Homola, *New approach to spectroscopy of surface plasmons.* Optics Letters, 2006. **31**(22): p. 3339-3341.
43. Slavik, R. and J. Homola, *Ultrahigh resolution long range surface plasmon-based sensor.* Sensors and Actuators B-Chemical, 2007. **123**(1): p. 10-12.
44. Homola, J., *Surface plasmon resonance sensors for detection of chemical and biological species.* Chemical Reviews, 2008. **108**(2): p. 462-493.
45. Besselink, G.A.J., et al., *Signal amplification on planar and gel-type sensor surfaces in surface plasmon resonance-based detection of prostate-specific antigen.* Analytical Biochemistry, 2004. **333**(1): p. 165-173.
46. Farre, M., et al., *Part per trillion determination of atrazine in natural water samples by a surface plasmon resonance immunosensor.* Analytical and Bioanalytical Chemistry, 2007. **388**(1): p. 207-214.
47. Schouten, H.F., et al., *Plasmon-assisted two-slit transmission: Young's experiment revisited.* Physical Review Letters, 2005. **94**(5).
48. Temnov, V.V., et al., *Surface plasmon interferometry: measuring group velocity of surface plasmons.* Optics Letters, 2007. **32**(10): p. 1235-1237.
49. Gay, G., et al., *The optical response of nanostructured surfaces and the composite diffracted evanescent wave model.* Nature Physics, 2006. **2**(4): p. 262-267.
50. Gay, G., et al., *Surface wave generation and propagation on metallic subwavelength structures measured by far-field interferometry.* Physical Review Letters, 2006. **96**(21).
51. Kim, T.J., et al., *Control of optical transmission through metals perforated with subwavelength hole arrays.* Optics Letters, 1999. **24**(4): p. 256-258.

52. Lee, M.H., H.W. Gao, and T.W. Odom, *Refractive Index Sensing Using Quasi One-Dimensional Nanoslit Arrays.* Nano Letters, 2009. **9**(7): p. 2584-2588.
53. Rigneault, H., et al., *Enhancement of single-molecule fluorescence detection in subwavelength apertures.* Physical Review Letters, 2005. **95**(11).
54. Bethe, *Theory of Diffraction by Small Holes.* Physical Review, 1944. **66**: p. 163.
55. Bouwkamp, C.J., *On Bethe's theory of diffraction by small holes.* Philips Research Reports, 1950. **5**: p. 321-322.
56. Degiron, A., et al., *Optical transmission properties of a single subwavelength aperture in a real metal.* Optics Communications, 2004. **239**(1-3): p. 61-66.
57. Grupp, D.E., et al., *Beyond the Bethe limit: Tunable enhanced light transmission through a single sub-wavelength aperture.* Advanced Materials, 1999. **11**(10): p. 860-+.
58. Degiron, A. and T.W. Ebbesen, *Analysis of the transmission process through single apertures surrounded by periodic corrugations.* Optics Express, 2004. **12**(16): p. 3694-3700.
59. Thio, T., et al., *Enhanced light transmission through a single subwavelength aperture.* Optics Letters, 2001. **26**(24): p. 1972-1974.
60. Shou, X., A. Agrawal, and A. Nahata, *Role of metal film thickness on the enhanced transmission properties of a periodic array of subwavelength apertures.* Optics Express, 2005. **13**(24): p. 9834-9840.
61. van der Molen, K.L., et al., *Influence of hole size on the extraordinary transmission through subwavelength hole arrays.* Applied Physics Letters, 2004. **85**(19): p. 4316-4318.
62. Wang, T.G., et al., *Study on electromagnetic wave transmission performances of ultra-thin metallic films.* Acta Metallurgica Sinica, 2005. **41**(8): p. 814-818.
63. Ghaemi, H.F., et al., *Surface plasmons enhance optical transmission through subwavelength holes.* Physical Review B, 1998. **58**(11): p. 6779-6782.
64. Barnes, W.L., et al., *Surface plasmon polaritons and their role in the enhanced transmission of light through periodic arrays of subwavelength holes in a metal film.* Physical Review Letters, 2004. **92**(10).
65. Porto, J.A., F.J. Garcia-Vidal, and J.B. Pendry, *Transmission resonances on metallic gratings with very narrow slits.* Physical Review Letters, 1999. **83**(14): p. 2845-2848.
66. Schouten, H.F., et al., *Light transmission through a subwavelength slit: Waveguiding and optical vortices.* Physical Review E, 2003. **67**(3).
67. Gordon, R., et al., *Basis and lattice polarization mechanisms for light transmission through nanohole arrays in a metal film.* Nano Letters, 2005. **5**(7): p. 1243-1246.
68. Chan, H.B., et al., *Optical transmission through double-layer metallic subwavelength slit arrays.* Optics Letters, 2006. **31**(4): p. 516-518.
69. Zayats, A.V. and I.I. Smolyaninov, *High-optical-throughput individual nanoscale aperture in a multilayered metallic film.* Optics Letters, 2006. **31**(3): p. 398-400.
70. Olkkonen, J., K. Kataja, and D.G. Howe, *Light transmission through a high index dielectric-filled sub-wavelength hole in a metal film.* Optics Express, 2005. **13**(18): p. 6980-6989.
71. Aouani, H., et al., *Large molecular fluorescence enhancement by a nanoaperture with plasmonic corrugations.* Optics Express, 2011. **19**(14): p. 13056-13062.

72. Krishnan, A., et al., *Evanescently coupled resonance in surface plasmon enhanced transmission.* Optics Communications, 2001. **200**(1-6): p. 1-7.
73. Janasek, D., J. Franzke, and A. Manz, *Scaling and the design of miniaturized chemical-analysis systems.* Nature, 2006. **442**(7101): p. 374-380.
74. Yager, P., et al., *Microfluidic diagnostic technologies for global public health.* Nature, 2006. **442**(7101): p. 412-418.
75. Craighead, H., *Future lab-on-a-chip technologies for interrogating individual molecules.* Nature, 2006. **442**(7101): p. 387-393.
76. Genet, C. and T.W. Ebbesen, *Light in tiny holes.* Nature, 2007. **445**(7123): p. 39-46.
77. Homola, J., *Present and future of surface plasmon resonance biosensors.* Analytical and Bioanalytical Chemistry, 2003. **377**(3): p. 528-539.
78. Anker, J.N., et al., *Biosensing with plasmonic nanosensors.* Nature Materials, 2008. **7**(6): p. 442-453.
79. Piliarik, M. and J. Homola, *Surface plasmon resonance (SPR) sensors: approaching their limits?* Optics Express, 2009. **17**(19): p. 16505-16517.
80. Okan, M., O. Balci, and C. Kocabas, *A microfluidic based differential plasmon resonance sensor.* Sensors and Actuators B-Chemical, 2011. **160**(1): p. 670-676.
81. Yanik, A.A., et al., *Integrated nanoplasmonic-nanofluidic biosensors with targeted delivery of analytes.* Applied Physics Letters, 2010. **96**(2).
82. Nenninger, G.G., et al., *Long-range surface plasmons for high-resolution surface plasmon resonance sensors.* Sensors and Actuators B-Chemical, 2001. **74**(1-3): p. 145-151.
83. Jan, C.M., Y.H. Lee, and C.K. Lee, *The Circular Polarization Interferometer based Surface Plasmon Biosensor.* Plasmonics in Biology and Medicine Vii, 2010. **7577**.
84. Wu, X.F., et al., *Refractive index sensor based on surface-plasmon interference.* Optics Letters, 2009. **34**(3): p. 392-394.
85. Braun, D. and P. Fromherz, *Fluorescence interferometry of neuronal cell adhesion on microstructured silicon.* Physical Review Letters, 1998. **81**(23): p. 5241-5244.
86. Dicken, M.J., et al., *Electrooptic Modulation in Thin Film Barium Titanate Plasmonic Interferometers.* Nano Letters, 2008. **8**(11): p. 4048-4052.
87. Duffy, D.C., et al., *Rapid prototyping of microfluidic systems in poly(dimethylsiloxane).* Analytical Chemistry, 1998. **70**(23): p. 4974-4984.
88. Temnov, V.V., et al., *Femtosecond surface plasmon interferometry.* Optics Express, 2009. **17**(10): p. 8423-8432.